Oncogene (2005), 1–12

www.nature.com/onc

ORIGINAL PAPER

topors, a p53 and topoisomerase I-binding RING finger protein, is a coactivator of p53 in growth suppression induced by DNA damage

Ling Lin[1,2,3], Toshinori Ozaki[4], Yuki Takada[1,2], Hajime Kageyama[4], Yoko Nakamura[4], Akira Hata[5], Jian-Hua Zhang[3], William F Simonds[3], Akira Nakagawara[4] and Haruhiko Koseki*[,1,2]

[1]*Department of Molecular Embryology, Graduate School of Medicine, Chiba University, 1-8-1 Inohana, Chuo-ku, Chiba 260-8670, Japan;* [2]*RIKEN Research Center for Allergy and Immunology, RIKEN Yokohama Institute, 1-7-22 Suehiro, Tsurumi-ku, Yokohama 230-0045, Japan;* [3]*Metabolic Diseases Branch, National Institute of Diabetes, Digestive and Kidney Diseases, NIH, Bethesda, MD 20892, USA;* [4]*Division of Biochemistry, Chiba Cancer Center Research Institute, 666-2 Nitona, Chuoh-ku, Chiba 260-8717, Japan;* [5]*Department of Public health, Graduate School of Medicine, Chiba University, 1-8-1 Inohana, Chuo-ku, Chiba 260-8670, Japan*

The RING family zinc-finger protein topors (topoisomerase I-binding protein) binds not only topoisomerase I, but also p53 and the AAV-2 Rep78/68 proteins. topors maps to human chromosome 9p21, which contains candidate tumor suppressor genes implicated in small cell lung cancers. In this study, we isolated the murine counterpart of topors and investigated its impact on p53 function. The deduced amino-acid sequence of mouse topors exhibits extensive similarity to human topors. Overexpressed myc-tagged topors associates with and stabilizes p53, and enhances the p53-dependent transcriptional activities of *p21*^{Waf1}, *MDM2* and *Bax* promoters and elevates endogenous *p21*^{Waf1} mRNA levels. Overexpression of topors consequently results in the suppression of cell growth by cell cycle arrest and/or by the induction of apoptosis. Taken together, these studies identify topors as a positive regulator of p53. The expression of *topors* is induced by exposure to the genotoxic reagents cisplatin and camptothecin, a DNA topoisomerase I inhibitor. We therefore postulate that topors mediates p53-dependent cellular responses induced by DNA damage, suggesting its physiological role as a tumor suppressor.
Oncogene advance online publication, 28 February 2005; doi:10.1038/sj.onc.1208554

Keywords: topors; p53; tumor suppressor; DNA damage; cell cycle; apoptosis

Introduction

The p53 tumor suppressor protein is defined as the guardian of the genome, and more than half of all human cancers are characterized by either the loss of the p53 protein or by mutations in its gene (Lane, 1992; Ko and Prives, 1996). The p53 protein comprises 393 amino acids including an amino-terminal transactivation domain, a sequence-specific DNA-binding domain and a multifunctional carboxyl-terminal domain. p53 is involved in the regulation of the cell cycle, apoptosis, senescence, DNA repair, cell differentiation and angiogenesis (Levine, 1997; Vogelstein *et al.*, 2000). These activities of p53 are mediated by one or more known mechanisms including the transcriptional regulation of target genes, functional regulation of interacting proteins, DNA annealing and exonuclease activity. p53 is activated by several stress conditions including DNA damage, the expression of several oncogene products, changes in cellular adhesion and redox potential, and reduction in the ribonucleoside triphosphate pool. In response to such stress signals, p53 undergoes extensive post-translational modification that modulates its stability and activity. The stabilization of p53 is presumed to play a major role in its activation, while modifications unrelated to p53 stabilization may regulate its specific activity (Sionov and Haupt, 1999; Vogelstein *et al.*, 2000). The stability of p53 is tightly regulated by multiple positive and negative feedback loops involving a number of p53 interacting proteins (Sionov and Haupt, 1999; Vogelstein *et al.*, 2000).

Human topoisomerase I-binding protein (h-topors) was first identified by yeast two-hybrid screening as a protein that interacts with human topoisomerase I (hTop1), and turned out to be identical to a novel p53-binding protein, p53BP3 (Haluska *et al.*, 1999; Zhou *et al.*, 1999). An identical protein was also isolated as the DNA-binding protein LUN, as a protein that interacts with adeno-associated virus type 2 (AAV-2) Rep78/68 proteins and as a protein binding to the interferon-inducible large GTPase Mx1 (Chu *et al.*, 2001; Engelhardt *et al.*, 2001; Weger *et al.*, 2002). h-topors is predicted to contain 1045 amino acids and to encode a RING family zinc-finger domain, a putative leucine zipper (LZ) domain, five sequences rich in proline, glutamine, serine and threonine (PEST sequences), an arginine/serine-rich (RS) domain and a bipartite nuclear localization signal (NLS). h-topors is

*Correspondence: H Koseki, RIKEN Research Center for Allergy and Immunology, RIKEN Yokohama Institute, 1-7-22 Suehiro, Tsurumi-ku, Yokohama 230-0045, Japan; E-mail: koseki@rcai.riken.jp
Received 1 June 2004; revised 18 January 2005; accepted 18 January 2005

modified by conjugation to the small ubiquitin-like modifier, SUMO-1 (Weger *et al.*, 2003), and both endogenous h-topors and overexpressed h-topors-GFP fusion protein are mainly distributed in promyelocytic leukemia-associated protein (PML) nuclear bodies in a PML protein-dependent fashion (Rasheed *et al.*, 2002). The carboxyl-terminal region of h-topors is required for such punctate nuclear localization (Rasheed *et al.*, 2002). In addition, the amino-terminal region of h-topors, containing the RING zinc-finger motif and LZ region, has been shown to bind to DNA in a sequence-specific as well as Zn^{2+}-dependent manner (Chu *et al.*, 2001). Since h-topors enhances the expression of a Rep78/68-dependent AAV-2 gene in the absence of helper virus, h-topors might be a transcriptional regulator (Weger *et al.*, 2002).

Although h-topors interacts with p53 as revealed by yeast two-hybrid assay, the role of h-topors in regulating the function of p53 remains to be clarified (Zhou *et al.*, 1999; Weger *et al.*, 2002). Several lines of evidence suggest that h-topors might be an important regulator in cell proliferation. Relocalization of topors in cells exposed to the Top1-targeting drug camptothecin (CPT) or the transcription inhibitor 5,6-dichloro-1-β-D-ribofuranolsylbenzimidazole (DRB) suggests its involvement in mediating the DNA damage response induced by CPT or DRB, which have been shown to cause an accumulation of p53 (Klibanov *et al.*, 2001; Rasheed *et al.*, 2002). h-topors interacts with AAV-2 Rep78, which has been proved to be an effective repressor of the adenovirus in the process of tumor generation (Schlehofer, 1994). Intriguingly, the region of h-topors required for interaction with AAV-2 Rep78/68 overlaps with that for p53 binding, as revealed by yeast two-hybrid analysis (Batchu *et al.*, 1999; Weger *et al.*, 2002). In addition, h-topors maps to chromosome 9p21, a locus containing candidate tumor suppressor gene(s) associated with the loss of heterozygosity in 86% of small cell lung cancers (Chu *et al.*, 2001). These observations prompted us to examine the functional role of topors in the regulation of p53. In the present study, we describe a physical and functional interaction between mouse topors and p53 in mammalian cultured cells. Our results strongly suggest that topors acts as a coactivator of p53 in response to DNA damage.

Results

Identification of a murine counterpart of topors

To identify proteins that interact with the Polycomb group (PcG) protein Mph2 (Yamaki *et al.*, 2002), we employed yeast-based two-hybrid screening using a cDNA library derived from mouse embryo and bait derived from full-length Mph2. We isolated two identical 1.2-kb cDNA fragments encoding a polypeptide highly homologous to the carboxyl-terminal half of h-topors. By conventional cDNA screening of a mouse brain cDNA library and database screening, two overlapping clones, a 3.5-kb fragment lacking the amino-terminal region and a mouse EST clone lacking the carboxyl-terminal region, were isolated. The nucleotide sequences of both clones were determined, and the combined nucleotide sequences revealed the longest open reading frame (ORF) of 1033 amino-acid residues with 86% overall identity to h-topors (DDBJ accession number: AB104865). In the amino-terminal region, a RING family zinc-finger domain and an LZ region exhibited 100 and 98% homology to h-topors, respectively (red letters and open blue box in Figure 1a, respectively). The p53-binding domains of h-topors were previously shown to be separated into two blocks based on yeast two-hybrid interactions (underlined in Figure 1a) (Zhou *et al.*, 1999; Weger *et al.*, 2002). A bipartite NLS was present in the amino-terminal block of the p53-binding domains (blue letters in Figure 1a). A cluster of residues including the two p53-binding subdomains and an intermediate region exhibited 90% identity with h-topors (Figure 1b). Because of the extensive similarity to h-topors, this newly isolated cDNA was identified as a murine counterpart of the *h-topors* gene. The mouse *topors* gene was mapped to a 40 Mb region of mouse chromosome 4 by BLAST analysis of the mouse genome (40017898–40007704 bp; Ensemble Mouse Genome Browser), a region syntenic to human chromosome 9p21. This chromosomal localization is in agreement with a previous report in which human *topors* was mapped to the chromosome 9p21 region (Chu *et al.*, 2001).

h-topors has been shown to associate with PML nuclear bodies in exponentially growing HeLa cells (Rasheed *et al.*, 2002). To examine the subcellular localization of mouse topors in mammalian cultured cells, we constructed an expression vector encoding myc-epitope-tagged topors (myc-topors) and confirmed its expression by *in vitro* transcription/translation experiments as well as transient transfection into COS-7 cells (Figure 1c and d). Consistent with the previous observation, myc-topors migrated more slowly (195 kDa) than predicted based on the calculated molecular mass, which has been suggested to be due to the phosphorylation of serine residues in the RS domain (Haluska *et al.*, 1999). The subcellular localization of myc-topors was also examined in U2-OS cells by transient overexpression. In interphase nuclei of morphologically intact transfectants, the myc-topors protein was always localized in the nuclei. Two types of transfectants were reproducibly observed. One type exhibited a fine speckled distribution to form 10–20 foci and the other type showed larger, closely spaced dots with much stronger fluorescence in the nucleoplasm but excluded from the nucleolus (data not shown). These findings were identical to those of Haluska *et al.* (1999), who described the subcellular localization of a GFP fusion with h-topors in HeLa cells.

topors interacts with p53 and enhances p53-dependent transcription in mammalian cultured cells

The putative p53-binding domains revealed by yeast two-hybrid interaction (Zhou *et al.*, 1999; Weger *et al.*,

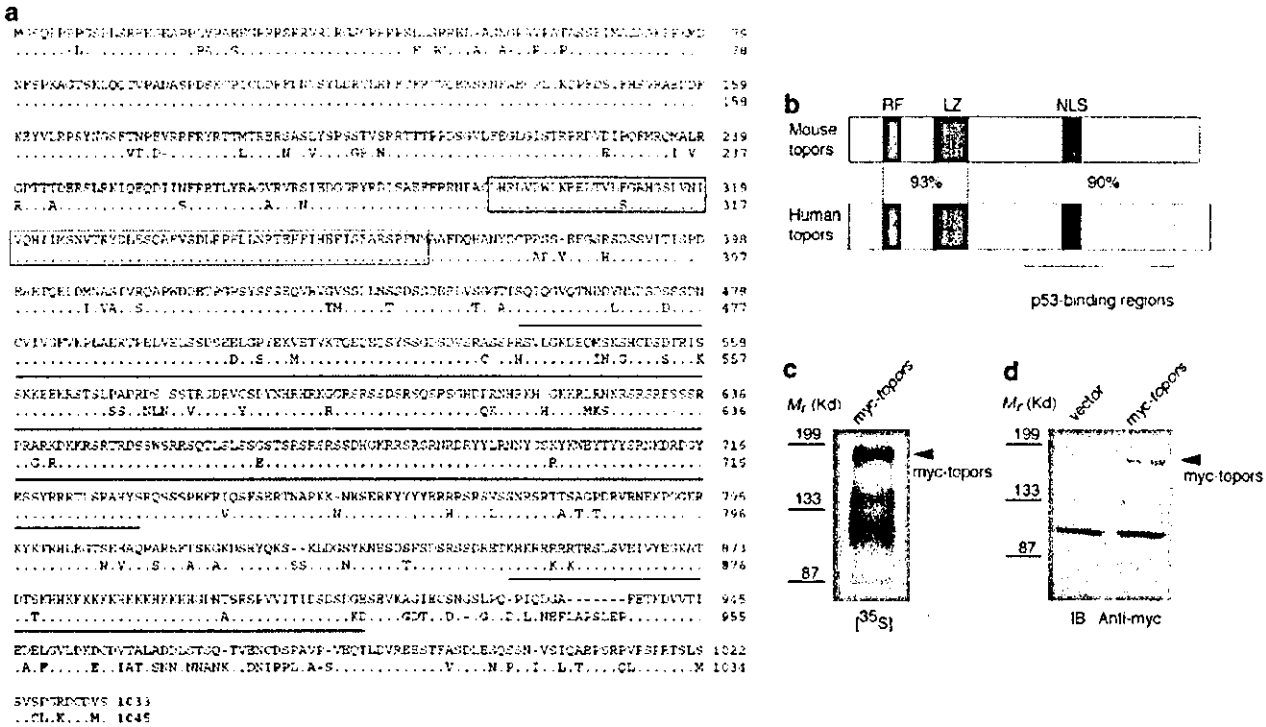

Figure 1 Amino-acid sequence, putative domain structure and expression of murine topors protein. (**a**) The deduced amino-acid sequence of mouse topors protein along with the sequence of the human counterpart. The sequences of mouse (top) and human (bottom) topors were aligned to provide the highest homology. Identical amino-acid residues are shown as dots in the human sequence; gaps are indicated by bars. Amino-acid residues in the putative RING finger motif and bipartite NLS are shown in red and blue letters, respectively. The region of the putative LZ structure is boxed with the hydrophobic residues at the first position of the heptad repeat shown in green letters. Two separate regions encoding putative p53-binding domains are underlined in red (see text). (**b**) Schematic representation of homologous domain structure shared between mouse and human topors. The RING finger motif (RF), LZ and bipartite NLS are indicated by red, green and blue boxes, respectively. Identical amino acids in each region are shown. (**c**) The myc-*topors* gene product generated by *in vitro* transcription/translation and analysed as described in Materials and methods. Relative molecular weight is indicated. (**d**) The myc-topors protein transiently overexpressed in COS-7 cells. Whole-cell lysates prepared from COS-7 cells transfected with either empty pcDNA3 (Vector, left) or pcDNA3-myc-*topors* (myc-*topors*, right) were subjected to immunoblotting analysis using the anti-myc monoclonal antibody

2002) are highly conserved between human and mouse topors (Figure 1a and b). This prompted us to examine whether myc-topors could interact with p53 in mammalian cultured cells. COS-7 cells were transiently transfected with myc-topors, and whole-cell extracts of the transfectants were subjected to immunoprecipitation with anti-p53 or normal mouse serum (NMS). As shown in Figure 2a, the anti-p53, but not the NMS, immunoprecipitates contained significant amounts of myc-topors, indicating that overexpressed myc-topors could associate with endogenous p53. This finding is consistent with the previous yeast two-hybrid studies demonstrating topors–p53 interaction (Zhou *et al*., 1999; Weger *et al*., 2002). We next addressed whether the physical interaction of topors with p53 might affect the function of p53. To this end, we examined the effects of overexpressed myc-topors on the p53-dependent transcription of *Bax*, *p21^{Waf1}* and *MDM2* promoters using luciferase assays in transiently transfected p53-deficient SAOS-2 and H1299 cells (Barak *et al*., 1993; el-Deiry *et al*., 1993; Miyashita and Reed, 1995). As shown in Figure 2b, the overexpression of myc-topors in SAOS-2 cells significantly enhanced p53-dependent transcription of the *Bax* and *MDM2* promoters in a dose-dependent manner. While myc-topors enhanced the p53-dependent activity of the *p21^{Waf1}* promoter in SAOS-2 cells, this effect did not achieve statistical significance (Figure 2b, middle panel). Similar results were obtained in H1299 cells, except that its effect on all three p53-responsive promoters was statistically significant as compared with p53 alone (Figure 2c). Under our experimental conditions, myc-topors alone had no effects on the *Bax*, *p21^{Waf1}* or *MDM2* promoter activity. We further studied whether the overexpression of topors influenced the expression of endogenous p53-regulated transcripts by quantitative real-time RT–PCR analysis of human *p21^{Waf1}* mRNA levels. As shown in Figure 2d and e, forced expression of topors enhanced the transcription of the p53 downstream gene *p21^{Waf1}* in both human small cell lung cancer SBC3 cells and U2-OS cells. Taken together, the results indicate that overexpression of topors enhances the sequence-specific transcriptional activity of p53 in a p53-dependent manner.

topors suppresses cell growth in a p53-dependent manner

These observations prompted us to investigate further whether the overexpression of myc-topors influences the growth suppression mediated by p53. For this purpose, we performed a colony formation assay using H1299 cells (lacking endogenous p53) and U2-OS cells containing the wild-type *p53* allele. The overexpression of myc-topors did not affect colony number in H1299 cells, while the colony number was significantly reduced in a dose-dependent manner in U2-OS cells (Figure 3a and b). The forced expression of p53 significantly reduced the colony number in H1299 cells, and this p53-dependent reduction was further intensified by cotransfection of pcDNA3-myc-*topors* (Figure 3a). Thus, the overexpression of topors appears to enhance the p53-dependent growth suppression of tumor cells.

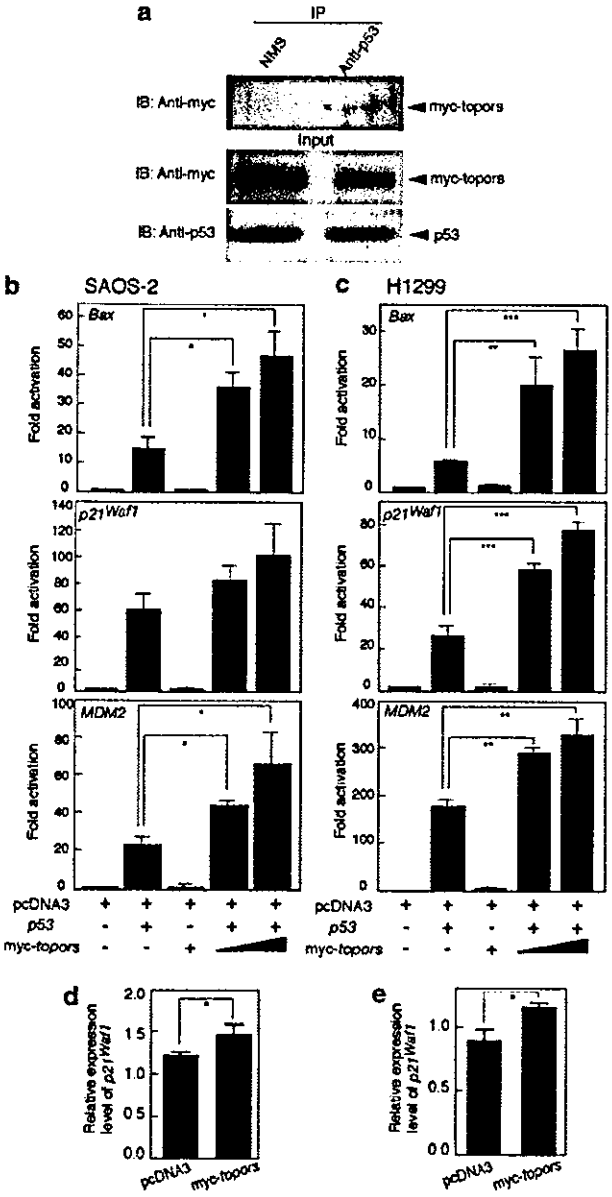

In different systems, p53 can induce apoptosis or cause cell cycle arrest (Ko and Prives, 1996; Vogelstein *et al*., 2000). Because topors was able to enhance p53-dependent growth suppression, we next examined whether topors-dependent growth suppression involves apoptosis. The number of apoptotic cells exhibiting nuclear condensation and fragmentation was counted 48 h after transfection with either pcDNA3-myc-*topors* or pEGFP (Figure 3c-I–III). The number of apoptotic cells increased significantly among U2-OS cells overexpressing myc-topors compared to pEGFP transfectants (Figure 3c-IV). Thus, the growth suppression resulting from overexpression of topors may result in part from induction of apoptosis.

Since p53 activation is known to cause not only apoptosis but also cell cycle arrest, we next examined the impact of overexpressed myc-topors on cell cycle progression. For this purpose, we established stable cell lines overexpressing myc-topors. U2-OS cells were transfected with pcDNA3-myc-*topors*, and G418-resistant clones were individually isolated and screened for myc-topors expression by immunofluorescent staining. Two cell lines out of 200 clones screened were found to express myc-topors (*topors* sta-1 and *topors* sta-2), and *topors* sta-1 expressed myc-topors at a higher level than *topors* sta-2 (Figure 4a). In both of the stable transfectants, myc-topors exhibited a speckled nuclear distribution to form 10–20 foci (Figure 4b), as did endogenous mouse topors in NIH 3T3 fibroblasts (data not shown) and as reported for endogenous human topors (Rasheed *et al*., 2002). *topors* sta-1 and *topors* sta-2 cells displayed a significantly slower growth rate

Figure 2 topors associates with p53 and activates p53-dependent transcription. (**a**) Association of transiently overexpressed myc-topors with endogenous p53 is shown by immunoprecipitation and subsequent immunoblotting analysis. (top) Whole-cell extract of COS-7 cells transfected with pcDNA3-myc-*topors* was subjected to immunoprecipitation with either NMS (left) or anti-p53 monoclonal antibodies (right) followed by immunoblotting with anti-myc monoclonal antibody. (middle and bottom) Unfractionated whole-cell extract of COS-7 cells transfected with myc-*topors* was subjected to immunoblotting using anti-myc monoclonal antibody (middle) or anti-p53 monoclonal antibody (bottom). (**b**, **c**) p53-deficient SAOS-2 (**b**) and H1299 (**c**) cells were transiently cotransfected with the expression plasmid for p53 along with luciferase reporter constructs containing the *Bax* (top), $p21^{Waf1}$ (middle) or *MDM2* (bottom) promoters in the presence or absence of increasing amounts of transfected pcDNA3-myc-*topors*. Transfection efficiency was standardized against *Renilla* luciferase. The average relative luciferase activities in triplicate experiments are represented as bars. Results are shown as fold induction of the luciferase activity compared with cells transfected with pcDNA3. Data shown are representative of two or three independent experiments with similar results. The significance of the differences was evaluated by Student's *t*-test (***$P<0.001$; **$P<0.01$; *$P<0.05$). (**d**, **e**) The expression of $p21^{Waf1}$ is upregulated by overexpression of myc-topors in small cell lung cancer cell SBC3 (**d**) and U2-OS cells (**e**). The expression of human $p21^{Waf1}$ was determined by quantitative real-time RT–PCR analysis as described in Materials and methods. Relative expression levels of $p21^{Waf1}$ were normalized to the levels of *β-actin* mRNA. The data shown are representative of two independent experiments with similar results. The significance of the differences was evaluated by Student's *t*-test (*$P<0.05$)

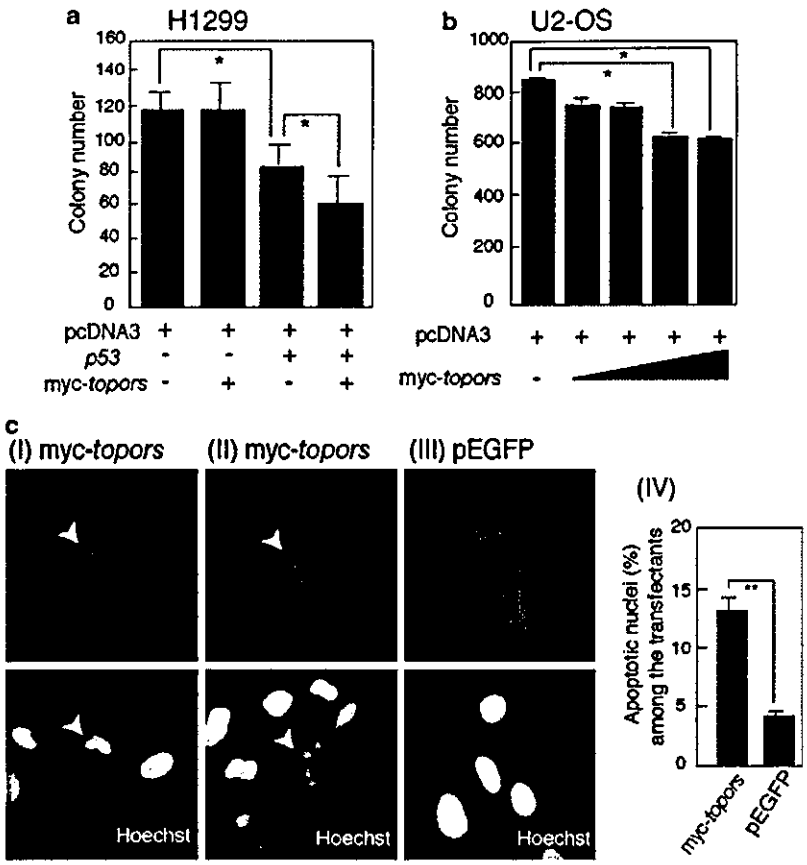

Figure 3 Enhancement of p53-dependent growth suppression and induction of apoptosis by the overexpression of topors. (**a**) The reduction in colony number by the transient overexpression of p53 is significantly enhanced by myc-topors in p53-deficient H1299 cells. (**b**) Increasing amounts of transfected myc-topors correlate with the reduction in colony number of U2-OS cells containing wild-type p53. Bars show the average numbers of colonies in triplicate experiments. The data shown are representative of three independent experiments with similar results. The significance of differences was evaluated by Student's *t*-test (*$P<0.05$). (**c**) Overexpression of myc-topors in U2-OS cells results in an increase in the number of apoptotic cells. U2-OS cells were transfected with either pcDNA3-myc-*topors* or pEGFP and transfected cells were identified by immunofluorescence staining with anti-myc monoclonal antibody or GFP expression, respectively (upper panels). Nuclear morphology was analysed after counterstaining with 1 μM Hoechst (lower panels). Cells overexpressing myc-topors frequently exhibit condensation (I) or fragmentation (II) of the nuclei, while GFP expression shows normal morphology (III). The percentages of apoptotic cells among >200 myc-topors- or GFP-positive cells were determined (IV). Values represent the means of three independent experiments. The significance of the differences was evaluated by Student's *t*-test (**$P<0.01$)

compared with the parental U2-OS cells and U2-OS cells transfected with empty vector (V-1) (Figure 4c). Of note, *topors* sta-1 cells grew more slowly than *topors* sta-2 cells, suggesting that the growth rate correlated inversely with the level of myc-topors expression in the respective cell lines. Next, asynchronous cultures of these transfectants and the parental cells were collected at 48 h after culture and their cell cycle distribution was analysed by flow cytometry. As shown in Figure 4d (cisplatin (−)) and e, *topors* sta-1 and *topors* sta-2 cells displayed a significant increase in the percentage of cells in G1 phase as compared with U2-OS and V-1 cells. A slight but reproducible increase in the sub-G1 fraction was seen exclusively in *topors* sta-1 cells (even without cisplatin treatment; see below), suggesting the constitutive occurrence of apoptosis in the *topors* sta-1 transfectants (Figure 4d and f (cisplatin (−))). The severe growth retardation of U2-OS cells stably expressing myc-topors might therefore result from both a prolonged G1 phase and a subtle induction of apoptosis. Comparison of the *topors* sta-1 and *topors* sta-2 results suggests that overexpression of topors can result in growth arrest and/or apoptosis depending on the degree of topors expression and the particular cellular context.

Stabilization of p53 by overexpression of topors

To determine whether the growth retardation produced by the stable overexpression of myc-topors was linked to the activation of p53, we next examined the expression of p53 and its response gene product, $p21^{Waf1}$ (Harper *et al*., 1993), in permanent transfectants. p53 was more abundantly expressed in both *topors* sta-1 and *topors* sta-2 stable transfectants than in control cell lines and the expression of $p21^{Waf1}$ was greater in both topors

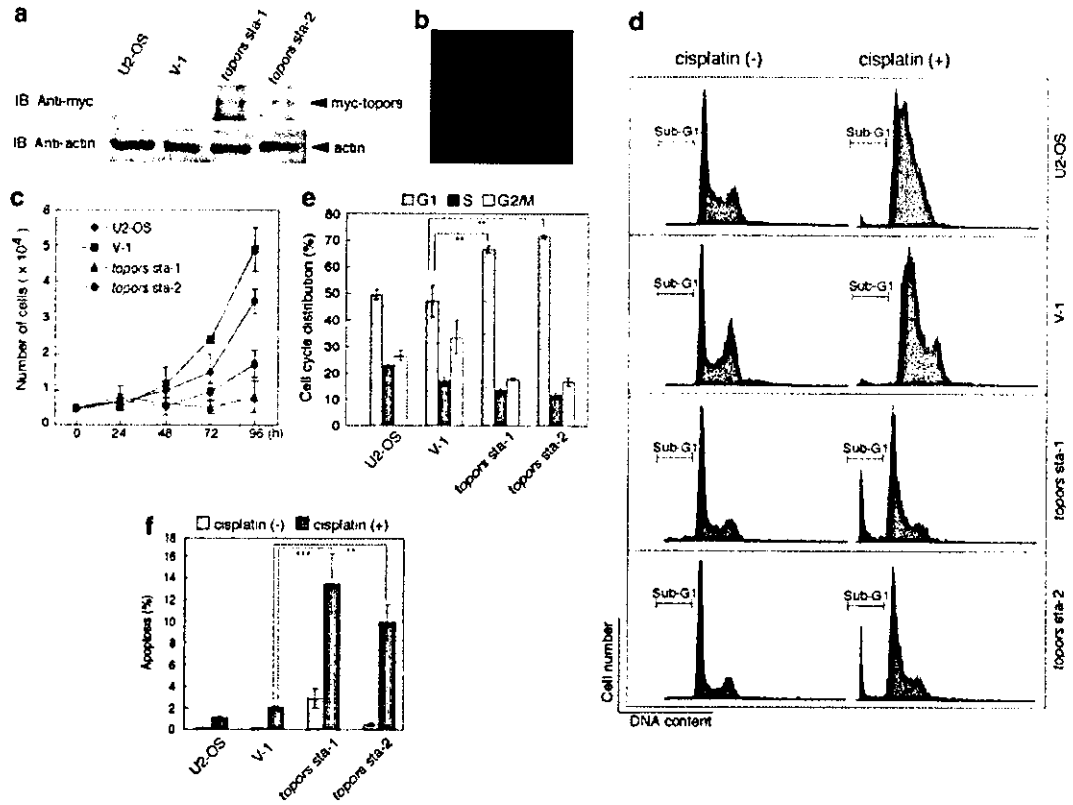

Figure 4 Cell cycle arrest and DNA damage-mediated apoptosis in U2-OS cells stably overexpressing myc-topors. (**a**) The expression of myc-topors in parental U2-OS cells and stable empty pcDNA3 vector (V-1) and pcDNA3-myc-*topors* (*topors* sta-1 and sta-2) transfectants as revealed by immunoblotting analysis using a polyclonal anti-myc antibody. The expression of actin is shown below as a loading control. (**b**) The expression pattern of myc-topors in *topors* sta-1 cell nuclei as revealed by immunofluorescent staining with anti-myc monoclonal antibody. (**c**) Growth rates of the indicated cells. The indicated cells were seeded at a density of 0.5×10^4 cells/well (12-well plate) and cell numbers were determined 1, 2, 3 and 4 days later. Average cell numbers at each time point determined in triplicate experiments are shown; standard deviations are shown in parentheses. Representative results of three independent experiments are shown. (**d**) Exponentially growing stable transfectants and control cells treated without or with cisplatin were stained with propidium iodide (PI) and subjected to FACS analysis. Representative FACS profiles of each cell line without (left) or with (right) cisplatin treatment are shown. Sub-G1 fractions are indicated. (**e**) Cell cycle profiles of exponentially growing U2-OS-derived cells as revealed by FACS analysis are shown by histograms. (**f**) Frequency of apoptotic cells among cells treated without (−) and with (+) cisplatin is shown by histograms. Values are the average percentages from triplicate experiments, and standard deviations are shown in parentheses. The experiments were repeated three times with essentially similar results. The significance of differences was evaluated by Student's *t*-test (***$P<0.001$; **$P<0.01$)

stable transfectants than in controls (Figure 5a). The increased level of $p21^{Waf1}$ protein correlated with the topors-enhanced expression of *p21*^{Waf1} mRNA in small cell lung cancer cells and U2-OS cells shown above (Figure 2d and e). Importantly, the upregulation of p53 and $p21^{Waf1}$ proteins in *topors* sta-1 was stronger than in *topors* sta-2, consistent with the relative expression level of ectopic myc-topors and the severity of the growth phenotypes in the two cell lines. The levels of expression of the p53 protein could also be increased by transient overexpression of myc-topors in U2-OS cells and p53-deficient large cell lung carcinoma H1299 cells, which were cotransfected with both FLAG-tagged *p53* and myc-*topors* (Figure 5c and d). Since the level of *p53* transcript was not significantly different in either of the permanent transfectants compared to controls (Figure 5b), it is likely that the increase in the amount of p53 protein was due to its stabilization. To investigate whether an increased protein half-life contributed to the elevated levels of p53 observed, we then determined the decay rate of p53 protein without and with topors overexpression. At 24 h after culture of the empty vector stable cells (V-1) and *topors* sta-2 cells, or 24 h post-transient transfection of p53-deficient human large cell lung carcinoma H1299 cells with FLAG-*p53* along with either pcDNA3 or pcDNA3-myc-*topors*, cells were treated with the protein synthesis inhibitor cycloheximide at a final concentration of 100 μg/ml for 0, 2, 4 and 6 h. The expression of p53 was then examined by immunoblotting for each time point and normalized by reference to the level of actin in each sample. As shown in Figure 5e, the p53 protein possessed a greater half-life in *topors* sta-2 cells compared with V-1 vector-transfected U2-OS cells. Similarly, the half-life of p53 was prolonged in the presence of topors compared to that of p53 cotransfected with pcDNA3 vector in p53-deficient

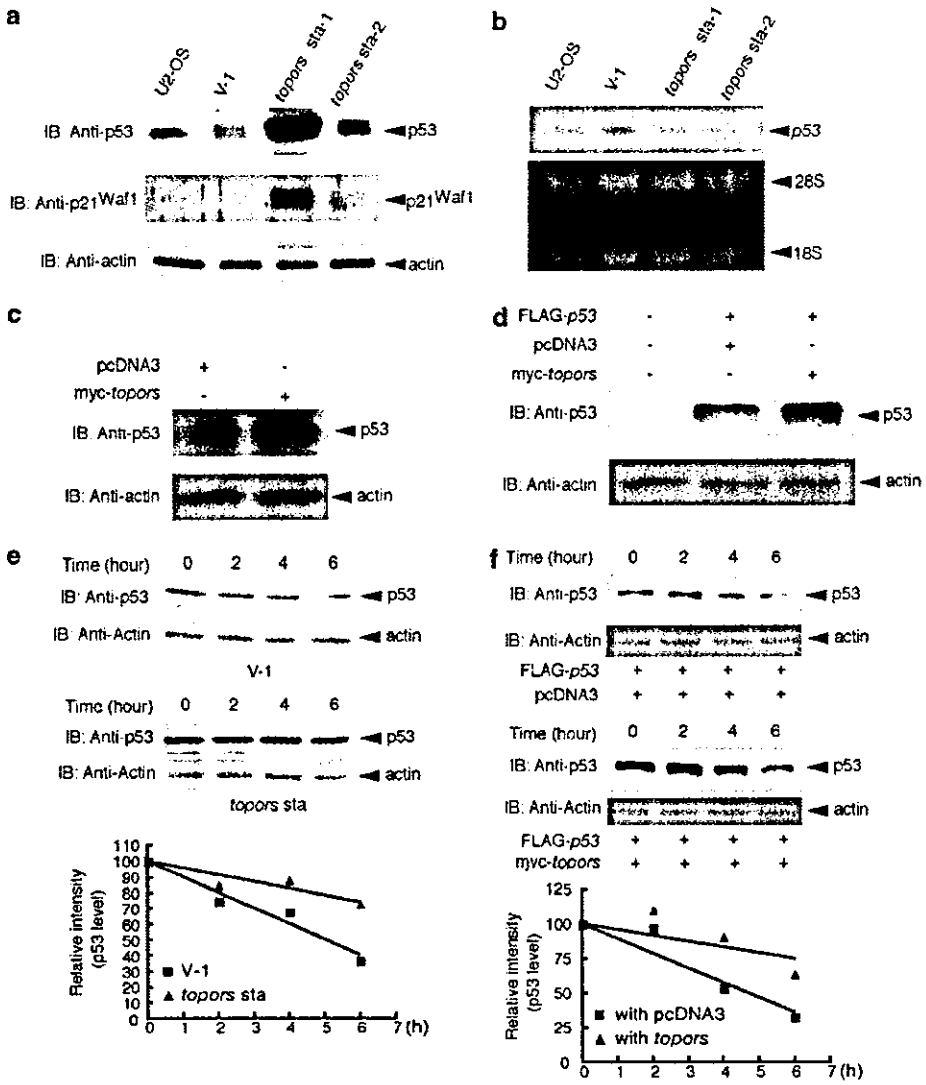

Figure 5 Stabilization of p53 protein by overexpression of myc-topors. (**a**) The expressions of p53 and $p21^{Waf1}$ in parental U2-OS cells and stable transfectants of pcDNA3 vector (V-1) and pcDNA3-myc-*topors* (*topors* sta-1 and sta-2) as revealed by immunoblotting analysis. The expression of actin is shown as a loading control. (**b**) The expression of *p53* transcript in each cell line as revealed by RNA blot analysis (upper panel). Ethidium bromide staining of 28S and 18S ribosomal RNA is shown as a loading control (lower panel). (**c**) The expression of p53 in U2-OS cells after transfection with pcDNA3 or pcDNA3-myc-*topors*. The expression of actin is shown as a loading control. (**d**) The expression of p53 in H1299 cells after transfection without or with FLAG-*p53* in the presence of pcDNA3 or pcDNA3-myc-*topors*. The expression of actin is shown as a loading control. (**e**, **f**) Increase in the half-life of p53 by topors. At 24 h after culture of pcDNA3 stable cells (V-1) and *topors* sta-2 cells (**e**), or at 24 h after transient transfection of p53-deficient H1299 cells (**f**) with expression plasmid of FLAG-*p53* along with pcDNA3 or pcDNA3-myc-*topors*, cycloheximide was added to the culture medium and the cells were extracted at the indicated time points. Whole-cell lysates were subjected to immunoblotting. The relative intensities of p53 were quantified by densitometric scanning, which normalized to actin, and are represented graphically

H1299 cells (Figure 5f). Taken together, these data suggest that expression of topors increases p53 levels by stabilizing p53 protein and thereby enhancing its ability to limit cell growth.

topors expression is induced by DNA damage

Our finding that transient or stable transfection of topors upregulates p53 levels suggests that topors could be a rate-limiting factor in the regulation of p53 function. If this is the case, a quantitative alteration of topors expression in a given cell could affect its apoptotic response to genotoxic reagents. To address this possibility, exponentially growing U2-OS cells or stable transfectants were treated with 20 μM cisplatin for 24 h, and the cells were then subjected to the cell cycle analysis. Following cisplatin treatment, both *topors* sta-1 and *topors* sta-2 cells demonstrated significantly increased sub-G1 fractions compared to the control cells (Figure 4d and f). The fraction of apoptotic cells among the *topors* sta-1 and *topors* sta-2 transfectants reached 80–90% after 48 h of cisplatin

treatment, compared to only 30–40% in control cells (data not shown). Thus, the overexpression of topors enhances the apoptotic response of U2-OS cells to DNA damage.

This finding suggests that upregulation of endogenous topors might be involved in mediating p53-dependent cellular responses to stress stimuli. We thus examined the expression of endogenous *topors* after cisplatin treatment in U2-OS cells. *topors* expression was obviously upregulated 24 and 48 h after cisplatin treatment consistent with the expression of p53 protein (Figure 6a). The analysis was extended to primary MEFs and C-20 cells, a mouse cell line derived from colon carcinoma. In these cells before treatment, *topors* was constitutively expressed while p53 was barely detectable. The apoptotic response of MEFs and C-20 cells to 20 μM cisplatin was more prominent than that of U2-OS cells (Figure 6b and c; compare to Figure 4d). The expression of the *topors* gene and p53 protein was increased in MEFs and C-20 cells by cisplatin treatment as well (Figure 6b and c). Since topors is a topoisomerase I-binding protein, we further investigated whether the expression of *topors* is also induced after treatment by CPT, a potent antineoplastic inhibitor of topoisomerase I (Haluska *et al*., 1999). As shown in Figure 6d, when U2-OS cells and NIH 3T3 cells were treated with CPT at the concentration of 10 μM, the expression of *topors* increased more than twofold compared to cells without treatment. However, it is still possible that the upregulation of *topors* mRNA might be a consequence of p53 induced during DNA damage-induced apoptosis. To exclude this possibility, we examined *topors* expression after overexpression of p53 by transient transfection. The overexpression of p53 did not significantly affect *topors* transcript levels (Figure 6e). Taken together, the induction of *topors* by the genotoxic reagents provides a mechanism to facilitate the p53-mediated DNA damage-dependent apoptosis in tumor and primary cells.

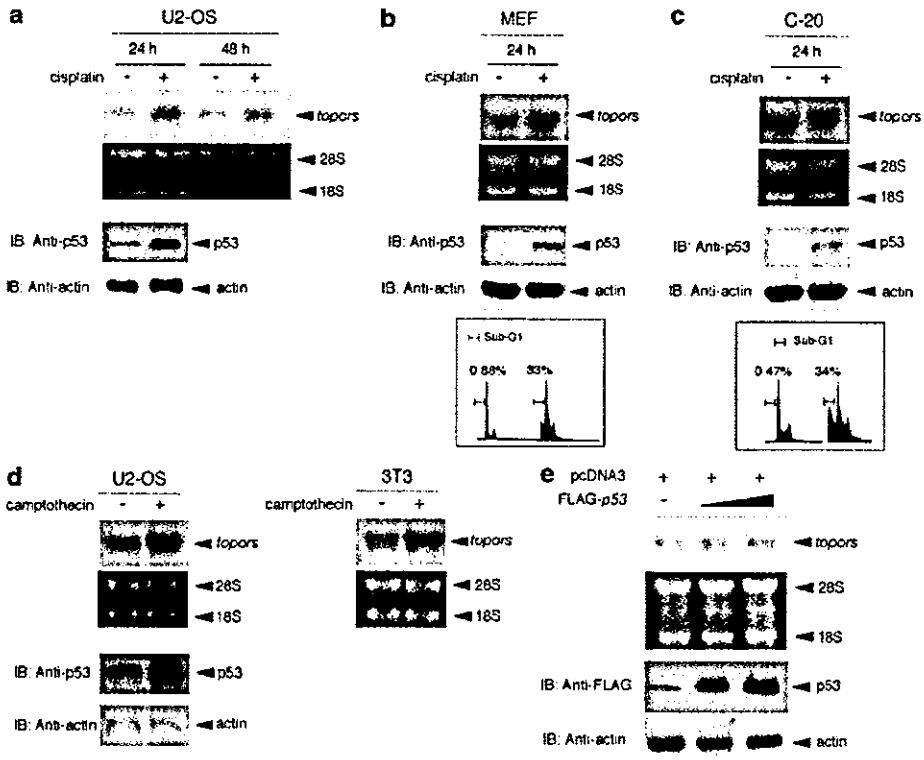

Figure 6 Induction of endogenous *topors* expression by DNA damage in human and mouse cell lines. (**a**) The expressions of *topors* and p53 are significantly induced in U2-OS cells in response to cisplatin treatment as revealed by RNA blot and immunoblotting analysis, respectively. (upper panels) *topors* transcripts detected as 4.0-kb bands (top) and ethidium bromide staining of 28S and 18S ribosomal as a loading control are shown (bottom). (lower panels) The expressions of p53 (top) and actin (lower) as a loading control are shown. (**b**, **c**) Induction of *topors* (upper panels), p53 expression (middle panels) and FACS analysis-based estimation of apoptosis (lower panels) by cisplatin treatment are also seen in primary MEFs (**b**) and murine colon carcinoma cells (C-20) (**c**). Percentages of cells in the sub-G1 fraction are shown in the lower panels. (**d**) The expressions of *topors* and p53 are significantly induced in U2-OS cells and NIH/3T3 cells in response to 12-h CPT treatment as revealed by Northern blot and immunoblotting, respectively. (upper panels) *topors* transcripts (top) and ethidium bromide staining of 28S and 18S ribosomal as a loading control are shown (bottom). (lower panel) The expressions of p53 (top) and actin (lower) as a loading control in U2-OS cells are shown. (**e**) The expression of *topors* is not affected by the transient overexpression of p53 in U2-OS cells. Increasing amounts of FLAG-*p53* documented by immunoblotting analysis (lower panels) do not significantly affect the expression of endogenous *topors* (upper panels). Ethidium bromide staining of 28S and 18S ribosomal RNA is shown as a loading control

Discussion

In the present study, we identify the mouse counterpart of human topors and document its involvement in p53-regulated cell growth control. Overexpressed topors associates with p53, activates p53-dependent transcription via the stabilization of p53 and, consequently, induces either cell cycle arrest or apoptosis in a dose-dependent manner. Therefore, our observations strongly implicate the topors protein as a novel coactivator of the p53 tumor suppressor protein.

We further show that expression of endogenous *topors*, as well as the p53 protein, is induced by DNA damage in tumor and primary cells. The present observations indicate that topors mediates p53-dependent cellular responses to some forms of DNA damage and, thus, could act as a tumor suppressor that activates p53. Interestingly, the human *topors* gene maps to chromosome 9p21 where the tumor suppressor genes associated with 86% of small cell lung carcinomas are suggested to reside and the above observations provide further evidence for the *topors* gene as a candidate tumor suppressor gene mapped to this region. Our preliminary studies have revealed that *topors* mRNA is expressed in all small cell lung cancer cell lines at levels similar to other tumor cell lines (L Lin and A Hata, unpublished data). Most recently, Oyanagi *et al.* (2004) revealed that the expression of *LUN* (*topors*) gene is downregulated in the development and metastases of lung cancer, suggesting that *LUN* might play important roles in inhibiting the oncogenesis of non-small cell lung cancer. The expression of topors protein in normal lung tissues and small cell lung cancers will require further future study.

The data clearly show that the overexpression of topors may cause either cell cycle arrest or apoptosis, and suggest that which occurs depends both on the topors level and the cellular context, although other variables require further exploration. There is a positive correlation between the amount of p53 protein and overexpressed topors in U2-OS cells in both transient and stable transfectants. Since it has repeatedly been reported that low levels of p53 expression are antiapoptotic while high levels promote apoptosis, high levels of topors could facilitate apoptosis due to the high level of p53 expression (Chen *et al.*, 1996; Lassus *et al.*, 1996). This phenomenon is further supported by another observation made in this study. We identified only two stable transfectants overexpressing myc-topors from 200 G418-resistant colonies and both exhibited a lower level of topors expression than that seen in the transiently transfected cells. This implies that only U2-OS cells overexpressing permissive amounts of exogenous topors might be allowed to survive by escaping apoptotic outbursts and instead exhibiting G1 cell cycle arrest, which is correlated with the induction of the downstream gene of p53, $p21^{Waf1}$. Interestingly, slight but significant apoptotic outbursts coincide with G1 arrest in *topors* sta-1, but not sta-2, cells. Slightly higher expression levels of myc-topors and, consequently, p53 in *topors* sta-1 cells than in sta-2 cells may be the cause for this phenotypical difference.

Our findings demonstrate that the expression level of topors protein may be a rate-limiting factor in the regulation of p53 activity. While this manuscript was in preparation, Saleem *et al.* (2004) also reported that transient expression of h-topors showed antiproliferative activity and was associated with G0/G1 cell cycle arrest in HeLa cells. Our results additionally show that overexpression of topors could activate the expression of p53 and induce either cell cycle arrest or apoptotic response.

In this study, we show that endogenous topors is significantly upregulated by the genotoxic reagents at the level of transcription in tumor and primary cells. A previous study has suggested that post-translational regulation of topors by DNA damage may also be involved (Rasheed *et al.*, 2002). In that study, overexpressed GFP-topors fusion protein immediately relocalized from PML nuclear bodies to the nucleoplasm in cells exposed to CPT or DRB. Since DRB exposure has also been shown to induce the accumulation of diffuse p53 in the nucleoplasm, it is possible that the relocalization of topors into the nucleoplasm might allow its association with and subsequent stabilization of p53 (Klibanov *et al.*, 2001).

The stability of the tumor suppressor p53 is crucial for its function to induce cell cycle arrest and/or apoptosis as a consequence of its ability to bind to specific DNA sequences and activate the transcription of adjacent genes (Vogelstein *et al.*, 2000). Overexpression of topors increased the stability of p53 and correspondingly enhanced the p53-dependent transcriptional activities. topors contains a RING finger motif, a domain that has been implicated in protein–DNA and protein–protein interactions, E2-dependent ubiquitination and SUMO conjugation (Kahyo *et al.*, 2001; Matthews and Sunde, 2002). Indeed, topors proteins have been recently shown to possess evolutionarily conserved E3 ubiquitin ligase activity. A *Drosophila* topors was shown to mediate Hairy polyubiquitination, resulting in Hairy, but not Dmp53 or topoisomerase I (dTopoI), degradation (Secombe and Parkhurst, 2004). Human GFP-topors fusion protein was shown to function as an E3 ligase for p53, albeit to a lesser degree than MDM2 (Rajendra *et al.*, 2004). Therefore, topors could affect the stability of p53 via covalent modification of p53 by ubiquitin isopeptide. This observation, however, is not necessarily consistent with our and others' previous observations suggesting topors as a likely tumor suppressor protein since polyubiquitination of p53 mediated by GFP-topors induces proteasome-dependent downregulation of p53 in U2-OS cells (Chu *et al.*, 2001; Rajendra *et al.*, 2004; Saleem *et al.*, 2004). This implies that regulation of p53 by topors may involve not only ubiquitination but also some other molecular mechanism.

Recently, the activity of p53 has been reported to be positively regulated by SUMO conjugation, which is mediated, at least in part, by another RING finger protein, PIAS (Gostissa *et al.*, 1999; Rodriguez *et al.*, 1999; Kahyo *et al.*, 2001). Sequence similarity between

two regions of topors and human PIASx protein, the RING domains and putative SUMO-1 interaction motifs suggests the possibility that topors may function as a SUMO E3 ligase (Weger *et al*., 2003). Indeed, h-topors and several components of SUMO-conjugating systems have been isolated together as interacting proteins with Mx1, an interferon-inducible GTPase that is associated with PML nuclear bodies (Engelhardt *et al*., 2001), which include p53, pRb, DAXX and CBP (Mann and Miller, 2004). Thus, topors may contribute to p53 stabilization or activation via SUMO conjugation processes.

The molecular mechanisms underlying the stabilization and/or activation of p53 by topors may also involve protein–protein interactions. AAV-2 Rep78/68 has been shown to possess a tumor suppressor property and to bind physically to p53 to prevent the adenovirus-mediated degradation of p53 (Batchu *et al*., 1999). Since topors is capable of interacting not only with p53, but also with Rep78/68, topors may cooperate with Rep78/68 to stabilize p53. It is possible that endogenous cellular regulators of p53 may function in ways analogous to these viral products and cooperate with topors to stabilize p53. These possibilities are not necessarily mutually exclusive. It will be essential to address experimentally the possible catalytic activities of topors.

Materials and methods

Isolation and preparation of an expression vector for a full-length cDNA of topors

Yeast two-hybrid screening was performed to isolate the cDNAs for Mph2-binding proteins from a cDNA library derived from E11.0 mouse embryo as described previously, and 177 independent clones were found to be positive for β-galactosidase activities as examined by filter assay (Vojtek *et al*., 1993; Kingma and Osheroff, 1998; Yamaki *et al*., 2002). The nucleotide sequences of the positive cDNA clones were determined. Two clones contained 1.2-kb cDNA fragments that were highly homologous to *h-topors* (Haluska *et al*., 1999). To isolate a full-length *topors* cDNA, a radiolabeled 1.2-kb cDNA fragment was used as a probe to screen the mouse brain cDNA library. After three rounds of hybridization, six positive clones were obtained and their nucleotide sequences were determined. The longest cDNA, containing a 3.5-kb insert, turned out to encode from the RING finger motif to the stop codon, but lacked a putative *topors* initiation codon. By searching public databases of mouse ESTs, we found a cDNA clone (MNCb-6014) that overlapped with the 3.5-kb cDNA clone. MNCb-6014, which was kindly provided by Dr Katsuyuki Hashimoto (Division of Genetic Resources, National Institute of Infectious Diseases, Japan), contained a *topors* initiation codon, but instead lacked the carboxyl-terminal region. To generate an expression vector encoding a full-length *topors*, the 5′-region of MNCb-6014 was amplified with primers 5′-CGTCGACAAGCTTATGGGGTCGCAGC CGCC-3′ (the *SalI*/*Hind*III restriction sites are underlined) and 5′-CAGAAGACAGTTCAACAAGTTCCGGGGTCC-3′ using the MNCb-6014 cDNA clone as a template. The PCR product was digested with *Sal*I and *Sph*I and subcloned into the identical restriction sites of the above-mentioned plasmid containing the 3.5-kb insert to produce a full-length cDNA for *topors* (pBluscript-M-*topors*). The pBluscript-M-*topors* was digested with *Hind*III and *Not*I and introduced into the identical restriction sites of pcDNA3-myc (Invitrogen, Carlsbad, CA, USA) to generate an expression vector for myc-tagged topors (pcDNA3-myc-*topors*).

In vitro *transcription/translation of the topors gene product*

The topors protein was generated from the pcDNA3-myc-*topors* vector using the T7-TNT Quick-Coupled Transcription–Translation system (Promega, Madison, WI, USA) in the presence of [^{35}S]methionine (Amersham Biosciences Inc., Piscataway, NJ, USA) according to the manufacturer's instructions. The quality of the synthesized protein was verified by electrophoresis though an 8% SDS–polyacrylamide gel and autoradiography.

Cell culture and transfection

Human osteosarcoma cell lines U2-OS and SAOS-2, COS-7, NIH/3T3 and primary MEFs were maintained in DMEM supplemented with 10% FBS and antibiotics. Human large cell lung carcinoma H1299 cells and human small cell lung cancer SBC3 cells were grown in RPMI-1640 medium supplemented with 10% FBS and antibiotics. All cells were cultured at 37°C in a water-saturated atmosphere of 5% CO_2 in air. COS-7 and U2-OS cells contain wild-type p53, while SAOS-2 and H1299 cells are deficient in p53 expression. For transfection, U2-OS cells were transfected by either the calcium phosphate co-precipitation method or Lipofectamine 2000 transfection reagent (Invitrogen, Grand Island, NY, USA) in accordance with the manufacturer's specifications. COS-7 cells were transfected with the FuGENE6 transfection reagent (Roche Molecular Biochemicals, Indianapolis, IN, USA). H1299 and SAOS-2 cells were transfected with the LipofectAMINE Plus transfection kit (Invitrogen, Grand Island, NY, USA) according to the manufacturer's protocol. To obtain stable transfectants, either pcDNA3 or pcDNA3-myc-*topors* was introduced into the exponentially growing U2-OS cells by the calcium phosphate co-precipitation method. At 48 h post-transfection, the cells were transferred to fresh medium containing G418 at a final concentration of 800 μg/ml. At 1 week after selection, drug-resistant colonies were isolated and the expression of myc-topors was examined by immunofluorescence staining as described below. As a control, a stable cell line of the pcDNA3 vector was established.

Immunoprecipitation and immunoblotting

Transfected cells were washed in ice-cold phosphate-buffered saline (PBS), lysed in lysis buffer (25 mM Tris-Cl, pH 7.5, 137 mM NaCl, 2.7 mM KCl, 1% Triton X-100 and 1 mM PMSF) and the extracts were sonicated briefly and centrifuged at 800*g* for 5 min to remove insoluble materials. The protein concentrations were determined by the Bradford protein assay (Bio-Rad, Hercules, CA, USA) using BSA as a standard. For immunoprecipitation, the cell lysates prepared from COS-7 cells transfected with pcDNA3-myc-*topors* were precleared using protein G-Sepharose beads at 4°C for 30 min under gentle rotation, and then incubated with either NMS or antibodies against p53 (DO-1, Oncogene Research Products, Cambridge, MA, USA and Pab1801, Santa Cruz Biotechnology Inc., Santa Cruz, CA, USA) at 4°C for 2 h. The immune complexes were then recovered with protein G-Sepharose beads. The immunoprecipitates or supernatants were subjected to SDS–polyacrylamide gel electrophoresis and electrophoretically transferred onto Immobilon P membranes (Millipore

Corp., Bedford, MA, USA). The membranes were blocked with TBS containing 0.1% Tween 20 and 5% nonfat dry milk, probed with antibodies against c-myc epitope (562, Medical and Biological Laboratories, Nagoya, Japan), p53 (DO-1, Oncogene Research Products, Cambridge, MA, USA), *p21^{Waf1}* (H-164, Santa Cruz), β-actin (20-33, Sigma Chemical Co., St Louis, MO, USA) and FLAG (M2, Sigma Chemical Co., St Louis, MO, USA), and then incubated with horse radish peroxidase-conjugated goat anti-rabbit or anti-mouse secondary antibody (Santa Cruz Biotechnology Inc., Santa Cruz, CA, USA). Immunoreactive bands were visualized with an ECL Western blot detection kit (Amersham Biosciences Inc., Piscataway, NJ, USA).

Immunofluorescence and confocal microscopy

Transfected cells grown on coverslips were fixed with 3.7% formaldehyde for 30 min at room temperature, permeabilized with 0.2% Triton X-100 for 5 min at room temperature and then incubated with 3% BSA in PBS for 2 h to reduce nonspecific antibody binding. Immunostaining was performed by incubating cells with a monoclonal anti-myc antibody (9E10, diluted 1:10) for 1 h at room temperature in a humidified chamber, followed by incubation with fluorescein isothiocyanate (FITC)-conjugated goat anti-mouse IgG (diluted 1:250) for 1 h at room temperature. The coverslips were washed extensively with PBS, mounted with PermaFluor (Immunon, Pittsburgh, PA, USA) and the labeled cells were examined using a confocal laser scan microscope (LSM510; Carl Zeiss Co., Ltd, Jena, Germany).

Luciferase reporter assay

SAOS-2 or H1299 cells were seeded at a density of 5×10^4 cells/well in a 12-well tissue culture dish and then cotransfected with 100 ng of p53/p73-responsive luciferase reporter constructs carrying *Bax*, *p21^{Waf1}* or *MDM2* promoter, 10 ng of pRL-TK and 25 ng of the p53 expression plasmid in either the presence or absence of increasing amounts of pcDNA3-myc-*topors* as described previously (Watanabe *et al*., 2002). The total amounts of DNA used in each transfection were kept constant (510 ng/transfection) using pcDNA3. Luciferase assays were performed 48 h post-transfection with a dual luciferase reporter assay system (Promega) according to the manufacturer's instructions.

Quantitative real-time RT–PCR analysis

Small cell lung cancer cell SBC3 and U2-OS cells were transfected with pcDNA3 or myc-*topors*. At 48 h after transfection, total RNA was extracted with the RNeasy Mini kit (Qiagen Inc., Valencia, CA, USA). Quantitative real-time RT–PCR was performed using the Brilliant SYBR Green QRT-PCR Master Mix Kit, 1-Step (Stratagene, La Jolla, CA, USA) and specific primers for human *p21^{Waf1}* and human *β-actin*. Quantitative results of *p21^{Waf1}* mRNA were normalized for the levels of *β-actin* mRNA. Specific primers for *p21^{Waf1}* are as follows: 5′-ATGAAATTCACCCCCTTTCC-3′ (forward primer) and 5′-CCCTAGGCTGTGCTCACTTC-3′ (reverse primer).

Colony formation assay

U2-OS and H1299 cells were transfected with pcDNA3 or pcDNA3-myc-*topors* in the presence or absence of FLAG-*p53* (a kind gift from Dr Toshiharu Suzuki, University of Tokyo, Tokyo, Japan). After 48 h of culture, the cells were divided into new dishes and cultured for 2 weeks in the presence of 400 μg/ml of G418. The cell dishes were fixed, stained with Giemsa's solution (Merck KgaA, 54271, Darmstadt, Germany, Art. 1.09204) and the colonies were counted.

Analyses of cell cycle and apoptosis

After treating cells with or without cisplatin (Sigma Chemical Co., St Louis, MO, USA) at a final concentration of 20 μM for 24 h, both floating and adherent cells were collected by brief centrifugation, fixed in 70% (v/v) ethanol for more than 4 h at −20°C and stained with PI (Sigma Chemical Co., St Louis, MO, USA). To identify cells with sub-G1 DNA content, the fluorescence of the nuclei was measured by flow cytometry (FACScan, Becton Dickinson, Oxford, UK). At least 5×10^4 events were analysed with Cell Quest software. For the morphological assessment of fragmented nuclei, U2-OS cells grown on coverslips were transfected with either myc-*topors* or pEGFP-N3 (BD Biosciences, CA, USA). At 48 h post-transfection, the cells were fixed with 3.7% formaldehyde, permeabilized with 0.2% Triton X-100 and blocked with 3% BSA in PBS. myc-topors was visualized with 9E10 monoclonal antibody (diluted 1:10) followed by FITC-conjugated goat anti-mouse IgG (diluted 1:250). DNA was visualized by incubating the cells with 1 mM Hoechst 33258 dye. Cells showing apoptotic morphological changes were analysed under a Leica QFluoro confocal spectral microscope (Leica Microsystems Imaging Solutions Ltd, Cambridge, UK).

Protein half-life determination

At 24 h after culture of the pcDNA3 stable cells (V-1) and *topors* sta-2 cells, or at 24 h post-transfection of p53-deficient human H1299 cells with FLAG-*p53* in combination with either pcDNA3 or pcDNA3-myc-*topors*, cycloheximide (Sigma) was added to the cell culture medium at a final concentration of 100 μg/ml. Cells were collected at the indicated time points and whole-cell extracts were subjected to immunoblot analysis with anti-p53 antibody. Best-fit linear regression analysis of the data points was performed with Prism 4.0 software (GraphPad).

Northern blot analysis

U2-OS cells, MEFs, C-20 cells and NIH/3T3 cells were cultured in the presence of cisplatin (20 μM) for 24 or 48 h or CPT (10 μM) for 12 h. Total cellular RNA was isolated using the Isogen kit (Wako Pure Chemical Industries, Ltd, Osaka, Japan). RNA (10 μg) was denatured in formaldehyde-formamide, separated by electrophoresis in 1.5% agarose gels and transferred to Hybond™-N+ membranes (Amersham Biosciences, Tokyo, Japan). The resulting blots were individually hybridized with radiolabeled probes specific for *topors* and *p53* at 65°C for more than 10 h. The filters were washed twice with 2 × SSC (300 mM NaCl and 30 mM sodium citrate, pH 7.0)/0.1% *N*-lauroyl sarcosine at room temperature for 30 min, and then once with 1 × SSC/0.1% *N*-lauroyl sarcosine at 55°C for 30 min.

Statistical analysis

Statistical analyses were performed using the unpaired Student's *t*-test. The differences between two groups were considered to be statistically significant when $P < 0.05$.

Acknowledgements
We are grateful to Dr M Vidal and Dr O Tetsu for critical reading of the manuscript, Dr O Ohara for providing the mouse cDNA library, Dr T Oda for providing the pBTM116

vector, Ms Sanae Takeda, Dr Jie Liu and Dr Tomomi Kaneko for kind assistance and Dr T Akasaka for initial instructions on yeast two-hybrid screening. This project was supported by a grant-in-aid for Scientific Research on Priority Areas and for Scientific Research (B) and Special Coordination Funds for Promoting Science and Technology from the Ministry of Education, Culture, Sports, Science and Technology of the Japanese Government to HK and AN.

References

Barak Y, Juven T, Haffner R and Oren M. (1993). *EMBO J.*, **12**, 461–468.
Batchu RB, Shammas MA, Wang JY and Munshi NC. (1999). *Cancer Res.*, **59**, 3592–3595.
Chen X, Ko LJ, Jayaraman L and Prives C. (1996). *Genes Dev.*, **10**, 2438–2451.
Chu D, Kakazu N, Gorrin-Rivas MJ, Lu HP, Kawata M, Abe T, Ueda K and Adachi Y. (2001). *J. Biol. Chem.*, **276**, 14004–14013.
el-Deiry WS, Tokino T, Velculescu VE, Levy DB, Parsons R, Trent JM, Lin D, Mercer WE, Kinzler KW and Vogelstein B. (1993). *Cell*, **75**, 817–825.
Engelhardt OG, Ullrich E, Kochs G and Haller O. (2001). *Exp. Cell Res.*, **271**, 286–295.
Gostissa M, Hengstermann A, Fogal V, Sandy P, Schwarz SE, Scheffner M and Del Sal G. (1999). *EMBO J.*, **18**, 6462–6471.
Haluska Jr P, Saleem A, Rasheed Z, Ahmed F, Su EW, Liu LF and Rubin EH. (1999). *Nucleic Acids Res.*, **27**, 2538–2544.
Harper JW, Adami GR, Wei N, Keyomarsi K and Elledge SJ. (1993). *Cell*, **75**, 805–816.
Kahyo T, Nishida T and Yasuda H. (2001). *Mol. Cell*, **8**, 713–718.
Kingma PS and Osheroff N. (1998). *Biochim. Biophys. Acta*, **1400**, 223–232.
Klibanov SA, O'Hagan HM and Ljungman M. (2001). *J. Cell Sci.*, **114**, 1867–1873.
Ko LJ and Prives C. (1996). *Genes Dev.*, **10**, 1054–1072.
Lane DP. (1992). *Nature*, **358**, 15–16.
Lassus P, Ferlin M, Piette J and Hibner U. (1996). *EMBO J.*, **15**, 4566–4573.
Levine AJ. (1997). *Cell*, **88**, 323–331.
Mann KK and Miller Jr WH. (2004). *Cancer Cell*, **5**, 307–309.
Matthews JM and Sunde M. (2002). *IUBMB Life*, **54**, 351–355.
Miyashita T and Reed JC. (1995). *Cell*, **80**, 293–299.
Oyanagi H, Takenaka K, Ishikawa S, Kawano Y, Adachi Y, Ueda K, Wada H and Tanaka F. (2004). *Lung Cancer*, **46**, 21–28.
Rajendra R, Malegaonkar D, Pungaliya P, Marshall H, Rasheed Z, Brownell J, Liu LF, Lutzker S, Saleem A and Rubin EH. (2004). *J. Biol. Chem.*, **279**, 36440–36444.
Rasheed ZA, Saleem A, Ravee Y, Pandolfi PP and Rubin EH. (2002). *Exp. Cell Res.*, **277**, 152–160.
Rodriguez MS, Desterro JM, Lain S, Midgley CA, Lane DP and Hay RT. (1999). *EMBO J.*, **18**, 6455–6461.
Saleem A, Dutta J, Malegaonkar D, Rasheed F, Rasheed Z, Rajendra R, Marshall H, Luo M, Li H and Rubin EH. (2004). *Oncogene*, **23**, 5293–5300.
Schlehofer JR. (1994). *Mutat. Res.*, **305**, 303–313.
Secombe J and Parkhurst SM. (2004). *J. Biol. Chem.*, **279**, 17126–17133.
Sionov RV and Haupt Y. (1999). *Oncogene*, **18**, 6145–6157.
Vogelstein B, Lane D and Levine AJ. (2000). *Nature*, **408**, 307–310.
Vojtek AB, Hollenberg SM and Cooper JA. (1993). *Cell*, **74**, 205–214.
Watanabe K, Ozaki T, Nakagawa T, Miyazaki K, Takahashi M, Hosoda M, Hayashi S, Todo S and Nakagawara A. (2002). *J. Biol. Chem.*, **277**, 15113–15123.
Weger S, Hammer E and Engstler M. (2003). *Exp. Cell Res.*, **290**, 13–27.
Weger S, Hammer E and Heilbronn R. (2002). *J. Gen. Virol.*, **83**, 511–516.
Yamaki M, Isono K, Takada Y, Abe K, Akasaka T, Tanzawa H and Koseki H. (2002). *Gene*, **288**, 103–110.
Zhou R, Wen H and Ao SZ. (1999). *Gene*, **235**, 93–101.

RESEARCH COMMUNICATION

Mammalian Polycomb-mediated repression of *Hox* genes requires the essential spliceosomal protein Sf3b1

Kyoichi Isono,[1] Yoko Mizutani-Koseki,[1] Toshihisa Komori,[2] Marion S. Schmidt-Zachmann,[3] and Haruhiko Koseki[1,4]

[1]Developmental Genetics Group, RIKEN Research Center for Allergy and Immunology, Tsurumi-ku, Yokohama 230-0045, Japan; [2]Department of Medicine III, Osaka University Medical School, Suita, Osaka 565-0871, Japan; [3]Division of Cell Biology, German Cancer Research Center, D-69120 Heidelberg, Germany

Polycomb group (PcG) proteins are responsible for the stable repression of homeotic (*Hox*) genes by forming multimeric protein complexes. We show (1) physical interaction between components of the U2 small nuclear ribonucleoprotein particle (U2 snRNP), including Sf3b1 and PcG proteins Zfp144 and Rnf2; and (2) that *Sf3b1*-heterozygous mice exhibit skeletal transformations concomitant with ectopic *Hox* expressions. These alterations are enhanced by *Zfp144* mutation but repressed by *Mll* mutation (a trithorax-group gene). Importantly, the levels of Sf3b1 in PcG complexes were decreased in *Sf3b1*-heterozygous embryos. These findings suggest that Sf3b1–PcG protein interaction is essential for true PcG-mediated repression of *Hox* genes.

Supplemental material is available at http://www.genesdev.org.

Received November 29, 2004; revised version accepted January 14, 2005.

During mammalian development, spatially and quantitatively appropriate homeotic (*Hox*) gene expression is essential for the anterior–posterior specification of axial structures (McGinnis and Krumlauf 1992; Duboule and Morata 1994). The maintenance of the *Hox* gene expressional state is driven by the products of Polycomb group (PcG) and trithorax group (trxG) genes (Satijn and Otte 1999; Francis and Kingston 2001; Simon and Tamkun 2002; Orlando 2003). In general, PcG proteins act as repressors to maintain the silent state, while the trxG proteins are activators that maintain *Hox* gene transcription. PcG proteins constitute large, chromatin-associated multiprotein complexes, which in mammals can be classified into at least two different classes. The Class I complex, which contains Eed/Ezh2, is associated with histone deacetylase and methyltransferase activity. The PRC1 or Class II complex consists of, for example, Zfp144 (Mel18), Rnf2 (Ring1B), Cbx2/M33, and Phc2/Edr2. The Class II complex, which characteristically includes the products from highly related pairs of genes, has been shown to inhibit nucleosome remodeling by the SWI/SNF complex in vitro (Shao et al. 1999). However, as the inhibition requires preincubation of the Class II with the nucleosomal template (it does not occur when Class II and SWI/SNF products are added together), this suggests that the Class II complex does not interact directly with SWI/SNF, but instead competes for the nucleosome template. Possibly, it is this binding of the Class II complex, which prevents nucleosome remodeling, that silences the genes by blocking the access of transcription activators to *cis*-regulatory elements such as promoters and enhancers (Francis et al. 2001). Interestingly, recent studies have proposed an alternative mechanism for maintaining gene silence (Breiling et al. 2001; Saurin et al. 2001). Fly Class II complex includes general transcription factors such as TBP and TBP-associated proteins at promoter regions. Using an in vitro assay, King et al. (2002) showed that the fly complex was able to inhibit transcription by RNA polymerase II at particular steps even after activator binding. This raises the possibility that the Class II complex might act directly on the functioning of the transcriptional machinery. However, whether this silencing mechanism is active at *Hox* loci during mammalian embryo development is not clear. In order to achieve a better understanding of the molecular basis of PcG complex-mediated repressions, we believe that it is important to identify PcG complex-associated non-PcG proteins and subsequently investigate the genetic impact of such proteins on PcG complexes. In this paper, we identified an essential spliceosomal protein Sf3b1 that physically interacts with the Class II PcG proteins and generated *Sf3b1* knockout mice. Surprisingly, *Sf3b1*$^{+/-}$ mice exhibited skeletal phenotypes that are usually observed with *PcG* mutation. Furthermore, genetic interactions between *Sf3b1* and *Zfp144* or the trxG gene *Mll* mutations were also shown. Therefore, it appears that Sf3b1 and the Class II PcG proteins are functionally interacting on the *Hox* loci in developing embryos.

Results and Discussion

Two partial cDNA clones encoding amino acid 1–489 and 312–777 regions of mouse spliceosomal protein Sf3b1 have been isolated as interactors for the mammalian PcG proteins Zfp144 and Rnf2, respectively, by yeast two-hybrid screening (Fig. 1A). Physical interactions between Sf3b1 and PcG proteins were first examined by glutathione S-transferase (GST) pull-down assay. Nuclear proteins were extracted from mouse embryonic stem (ES) cells and subsequently precipitated by GST–Rnf2 and GST–Zfp144 fusion proteins. The precipitates were subjected to immunoblotting with anti-Sf3b1 antibody. Endogenous Sf3b1 was clearly coprecipitated with GST–Rnf2 and GST–Zfp144 (Fig. 1B). Moreover, assay with Rnf2 truncates revealed that Sf3b1 specifically in-

[*Keywords*: *Hox* genes; Polycomb group; knockout mice; spliceosomal proteins]
[4]Corresponding author.
E-MAIL koseki@rcai.riken.jp; FAX 81-45-503-9690.
Article and publication are at http://www.genesdev.org/cgi/doi/10.1101/gad.1284605.

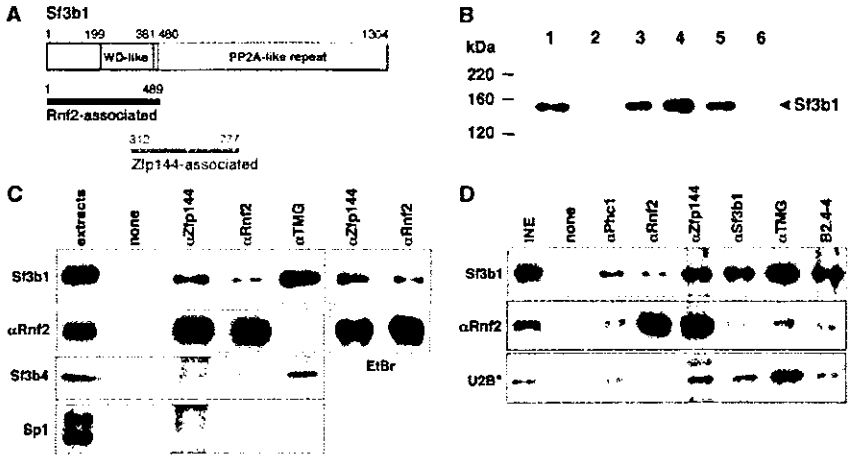

Figure 1. Physical interaction between Sf3b1 and PcG proteins. (*A*) Primary structure of Sf3b1 (Isono et al. 2001). Sf3b1 has WD-40 like repeats and PP2A repeats (usually termed HEAT motifs) originally identified in the PR65 subunit of protein phosphatase 2A. The N-terminal region (amino acids 1–489) and the internal region (amino acids 312–777), respectively, were associated with Rnf2 and Zfp144 in the yeast two-hybrid system. (*B*) GST pull-down assays probed with the Sf3b1-specific antibody. Nuclear extracts from ES cells were incubated with GST alone (lane *2*) and GST fusions with Zfp144 (lane *3*), Rnf2 (lane *4*), and the N-terminal (lane *5*) or C-terminal (lane *6*) regions of Rnf2. In lane *1*, one-fifteenth volume of extract sample used in a reaction was applied. (*C*) Coimmunoprecipitation with whole-cell lysates. Lysate of a mouse embryo at 10.75–11.25 dpc was incubated with or without antibodies to Zfp144, Rnf2, or TMG. Each precipitant was divided into two, and each was used in immunoblotting with Sf3b1 and Rnf2 or Sp1 and Sf3b4 antibodies. Anti-Sp1 was used as a negative control. In each "extract" lane, one-fortieth volume of extract sample used in a reaction was applied. In addition, lysates treated with ethidium bromide (EtBr) were also used to exclude DNA. (*D*) Coimmunoprecipitation with chromatin-rich lysates. Insoluble nuclear extract from an embryo at 10.75–11.25 dpc was prepared by osmotic shock, solubilized by sonication, and then incubated with antibodies. Phc1 is a mouse homolog to the fly PcG protein, Polyhomeotic (the fly protein homologous to mouse Phc1). B2.4-4 is a polyclonal antibody against the *Xenopus* Sf3b1, which has an epitope different from the monoclonal antibody (αSf3b1). In the "INE" lane, one-fortieth volume of the insoluble extract used in a reaction was applied.

teracts with the N-terminal region (amino acids 1–188) but not with the C-terminal region (amino acids 189–336). Thus, Sf3b1 probably has the potential to bind directly to Rnf2 and Zfp144.

We examined the in vivo interaction further in whole-cell extracts from 11.5 d post-coitus (dpc) embryos in which PcG complexes have been shown to act as repressors of *Hox* gene expression (Fig. 1C; Akasaka et al. 1996). A significant, but substoichiometric amount, of Sf3b1 was reproducibly coimmunoprecipitated with Zfp144 and Rnf2, as revealed by comparison with anti-Rnf2 immunoblotting. The presence of ethidium bromide did not affect these Sf3b1–Zfp144/Rnf2 interactions, which suggests that they were DNA independent. As Sf3b1 is known to be a component of U2 snRNP (Krämer 1996; Schmidt-Zachmann et al. 1998), we therefore examined other U2 snRNP components, Sf3b4 (SAP49), U2B", and U snRNAs. In the conventional nuclear extracts, Sf3b4 was also coprecipitated with PcG proteins while anti-2,2,7-trimethylguanosine (TMG) antibody, which reacts to the 5′ cap of U snRNAs characteristic for the U1, U2, U5, and U4/U6 snRNPs (Krämer 1996), failed to coprecipitate Rnf2. It is, however, possible that excess nucleoplasmic spliceosomal proteins or nucleoplasmic interaction between monomeric Sf3b1 and the PcG proteins would obscure experimental outcomes. To exclude these possibilities, we employed nuclear insoluble fraction extracted under high salt condition, in which proteins closely associated to chromatin are presumed to be concentrated. The fractions were solubilized by sonication and used in immunoprecipitation. Coimmunoprecipitation of Rnf2 with Phc1/Rae28 and Zfp144 indicated the presence of PcG multimeric complexes in this fraction. Sf3b1 and U2B" were coimmunoprecipitated with Phc1, Rnf2, and Zfp144. Concordantly, two different anti-Sf3b1 antibodies were able to coimmunoprecipitate Rnf2, reinforcing the interaction between Sf3b1 and PcG proteins. Notably, significant amounts of Rnf2 as well as Sf3b1 and U2B" were coimmunoprecipitated by anti-TMG antibody, implying the association of the U2 snRNA to PcG complexes. Importantly, these U2 snRNP components bound to the PcG proteins were detected in similar proportions (Fig. 1C,D). Taken together, these results show that it is likely that PcG complexes associate with at least part of the U2 snRNP rather than Sf3b1 alone.

To examine the biological implications of *Sf3b1*, we have generated an *Sf3b1*-mutant allele by replacing four exons with the *neo* gene in the opposite direction. *Sf3b1* null homozygotes died during preimplantation development around the 16- to 32-cell stage. Heterozygotes were externally normal and healthy, although the levels of *Sf3b1* mRNA and Sf3b1 were significantly reduced (Supplementary Fig. S1). Since *PcG* mutants exhibit posterior transformations of the vertebrae (Akasaka et al. 1996; Gould 1997; Suzuki et al. 2002), we examined axial skeletal preparations of $Sf3b1^{+/-}$ newborn pups backcrossed five times (N5) to C57BL/6 background. Significantly, $Sf3b1^{+/-}$ mice exhibited various skeletal alterations along the anterior–posterior axis (Table 1). In the cervical region of $Sf3b1^{+/-}$ mutants, the seventh cervical vertebra (C7) had incomplete ectopic ribs, either unilaterally or bilaterally fused with the first thoracic rib (27%), indicating transformations of C7 toward the first thoracic vertebra (T1) (Fig. 2B). Twenty-nine percent of $Sf3b1^{+/-}$ mutants had a prominent spinous process, characteristic for the second thoracic vertebra (T2), incorrectly associated with T1 (Fig. 2C), suggesting a T1 → T2

Table 1. *Summary of skeletal transformations in mutant mice*

Parents	B6 × *Sf3b1*$^{+/-}$ (N4)		*Mel18*$^{+/-}$ × *Sf3b1*$^{+/-}$ (N4)				*Mll*$^{+/-}$ × *Sf3b1*$^{+/-}$ (N6)			
Transformation types	wt (*n* = 50)	*Sf3b1*$^{+/-}$ (*n* = 48)	wt (*n* = 21)	*Mel18*$^{+/-}$ (*n* = 18)	*Sf3b1*$^{+/-}$ (*n* = 22)	*Mel18*$^{+/-}$*Sf3b1*$^{+/-}$ (*n* = 20)	wt (*n* = 14)	*Mll*$^{+/-}$ (*n* = 23)	*Sf3b1*$^{+/-}$ (*n* = 25)	*Mll*$^{+/-}$*Sf3b1*$^{+/-}$ (*n* = 15)
C7 → T1	0 (0)	27 (13)	0 (0)	6 (1)	32 (7)	45 (9), [a]4/9	0 (0)	0 (0)	68 (17)	0 (0)
T1 → T2	0 (0)	29 (14)	0 (0)	11 (2)	23 (5)	75 (15)	7 (1)	0 (0)	60 (15)	0 (0)
T13 → L1	0 (0)	6 (3)	0 (0)	28 (5)	14 (3)	50 (10)	0 (0)	9 (2)	8 (2)	13 (2)
L6 → S1	22 (11)	88 (42)	62 (13)	89 (16)	100 (22)	100 (20)	21 (3)	61 (14)	88 (22)	87 (13)

[a]Four out of nine C7 → T1 mice exhibited complete first ribs associated with the C7 vertebra (see Fig. 2G).
Unit: % (*n*).

transformation. In addition, *Sf3b1*$^{+/-}$ mice had only 12 ribs (6%) (Fig. 2F) and five lumbar vertebrae (88%) (Fig. 2E–F), indicating T13 → L1 and L6 → S1 transformations, respectively. Thus, *Sf3b1*$^{+/-}$ mice exhibit skeletal phenotypes similar to *PcG* mutants although the penetrance is rather low. We investigated next whether these skeletal alterations, seen with *Sf3b1*$^{+/-}$, were associated with anterior shifts of *Hox* gene expression boundaries as well as *PcG* mutants (Akasaka et al. 1996). The *Hoxb8* expression was extended to the seventh prevertebrae in three out of five *Sf3b1*$^{+/-}$ embryos and from the eighth prevertebra in wild type (Fig. 2L–N), and also *Hoxb6* and *Hoxc6* were ectopically expressed in the sixth prevertebrae in *Sf3b1*$^{+/-}$ embryos (Fig. 2I–K,O–Q). Significant changes were not observed for *Hoxa5*, *Hoxb3*, *Hoxb4*, or *Hoxd4* expression in the paraxial me-

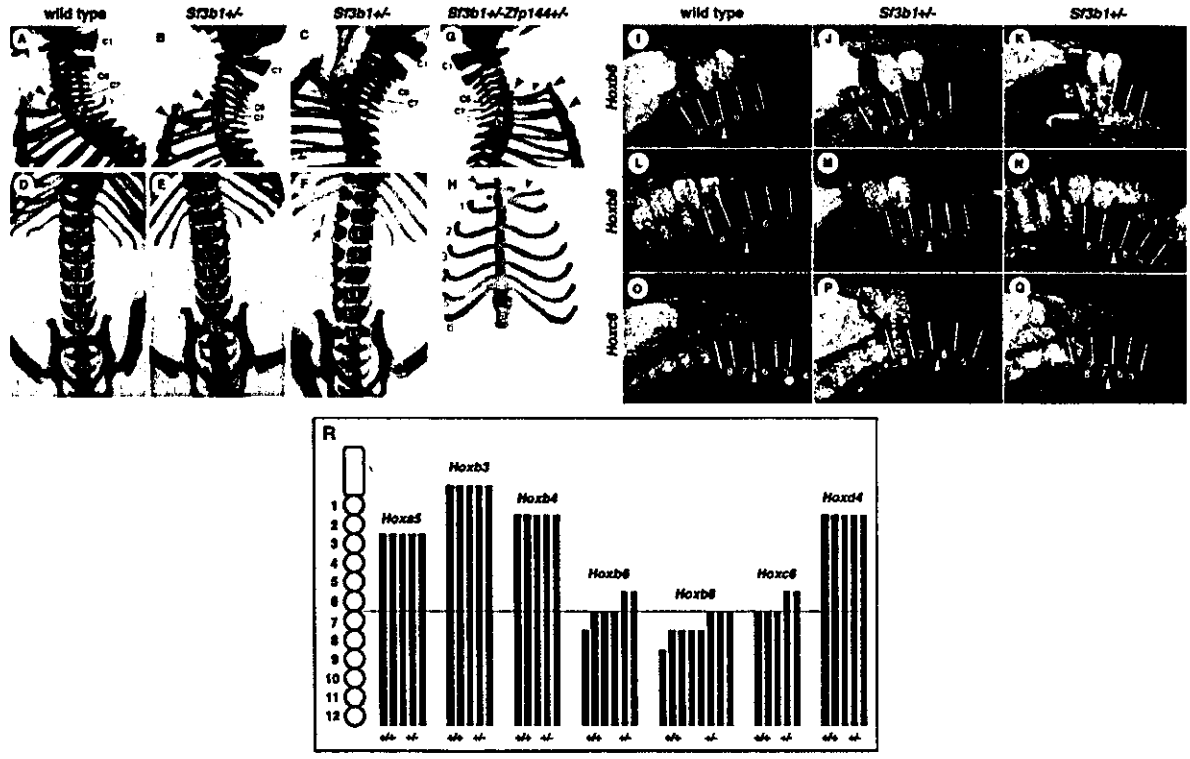

Figure 2. Skeletal abnormalities and ectopic *Hox* expressions in *Sf3b1*$^{+/-}$ mice. Cervical–thoracic (lateral view) and thoracic–sacral (ventral view) regions of wild-type (*A,D*) and two independent *Sf3b1*$^{+/-}$ (*B,C,E,F*) newborns are shown. Numbering of vertebrae of mutants makes them consistent with those of wild type. In wild type, C6 and T2 vertebrae have characteristic ventral processes as indicated by arrowheads (orange) and a prominent spinous process (yellow circle), respectively. An arrow indicates the disappearance of the T13 rib in the *Sf3b1*$^{+/-}$ mutant. (*G,H*) the lateral view of cervical–thoracic region and the ventral view of rib cage of the *Sf3b1*$^{+/-}$*Zfp144*$^{+/-}$ compound mutant. Ectopic ribs with C7 are represented by black arrowheads. An asterisk indicates an additional ossification center. Ribs numbered as 1–6 associate with T1–T6 vertebrae, respectively. The right ectopic rib with C7 separates from the rib with T1 on the sternum, as shown by green arrowheads. (*I–Q*) RNA in situ hybridization of *Hox* genes in embryos at 11.5 dpc. Boundaries of prevertebrae in lateral view are indicated by lines and the prevertebrae are numbered from prospective C1. Vertebral arteries are indicated by arrowheads and anterior boundaries of expressions are indicated by arrows. In *Sf3b1*$^{+/-}$ embryos, anterior boundaries of *Hoxb6*, *Hoxb8*, and *Hoxc6* expressions are shown to shift by sixth, seventh, and sixth prevertebrae, respectively. (*R*) Summary of *Hoxa5*, *Hoxb3*, *Hoxb4*, *Hoxb6*, *Hoxb8*, *Hoxc6*, and *Hoxd4* expressions in the paraxial mesoderm is depicted schematically. Each black (wild type) or gray (*Sf3b1*$^{+/-}$) bar represents expressional regions and a number of bars show individual embryos. Segment numbers are counted from the prospective C1.

soderm of *Sf3b1*$^{+/-}$ embryos (Fig. 2R). However, we found a subtle alteration of the *Hoxd4* expression in the second branchial arch of *Sf3b1*$^{+/-}$ embryos (data not shown). In summary, the expressions of several *Hox* genes were anteriorly extended in the paraxial mesoderm and second branchial arch in *Sf3b1*$^{+/-}$ embryos. These observations are consistent with the axial skeletal alterations observed in *Sf3b1*$^{+/-}$ mice. Therefore, we concluded that Sf3b1 mediates the repression of *Hox* genes.

Individual *PcG* mutations have been shown to mutually enhance their phenotypes (Bel et al. 1998; Akasaka et al. 2001; Suzuki et al. 2002). To investigate whether this Sf3b1-mediated repression involves PcG complexes, we examined the genetic interactions between *Zfp144* and *Sf3b1* mutations. In *Sf3b1*$^{+/-}$*Zfp144*$^{+/-}$ double heterozygotes, the formation of an additional ossification center in the sternum, and the detachment of the ribs of T7 from the sternum, represented an anterior shift of the sternum of one segment width (Fig. 2H). The ectopic ribs associated with C7 mimicked perfect ribs and formed joints with the anteriorly shifted sternum (Fig. 2G). These alterations were observed in four (44%) out of nine double mutants that displayed perfect C7 → T1 transformation but were not observed in either of the single mutants (Table 1). In addition to the ectopic ribs, the frequencies of other transformations were much higher in the double mutants. In particular, the T1 → T2 transformation occurred at a much higher penetrance: 75% in double mutants versus only 11% or 23% in either single mutant, suggesting that the single phenotypes of respective mutations were enhanced in the presence of each other. We further examined the impact of the *Sf3b1* mutation on the mutation at the *mixed lineage leukemia* (*Mll*) gene (Yu et al. 1995), a mammalian homolog of the *trithorax* gene of *Drosophila melanogaster*, whose product is antagonistic to *PcG* mutations (Hanson et al. 1999). Posterior transformations at the cervico–thoracic transitional zone caused by *Sf3b1* mutation were completely restored by *Mll* mutation (Table 1; Yagi et al. 1998). Therefore, it is likely that Sf3b1 has an antagonistic relationship to trxG proteins as well as PcG complexes. Taken together, these results indicate that Sf3b1 is functionally involved in PcG repressive complexes.

Since Sf3b1 is involved essentially in pre-mRNA splicing, the basal expression levels of genes, including *PcG* or *Hox* genes, may be profoundly altered in *Sf3b1*$^{+/-}$ mice, leading to homeotic transformations. To investigate this, a basal activity of splicing was examined with nuclear extracts from 10.5 dpc *Sf3b1*$^{+/-}$ embryos in which the Sf3b1 level was reduced up to ~75% but Rnf2 accumulated at normal level (data not shown). Despite such lower quantities of Sf3b1, their splicing activity was equal because of the same ratio of their spliced forms (Fig. 3A). Furthermore, while expression levels of *Sf3b1* were reduced by half in *Sf3b1*$^{+/-}$ embryos, those of five PcG genes, *Zfp144*, *Rnf2*, *Eed*, *Cbx2/M33*, and *Phc2/Edr2*; three *Hox* genes, *Hoxb3*, *Hoxb6*, and *Hoxb8*; and a metabolic gene, *Hprt*, were not (Fig. 3B). Thus, homeotic transformations in *Sf3b1*$^{+/-}$ mice appear to be independent of the alteration of general gene expression. Next, we investigated the amount of Sf3b1 associated with PcG proteins in *Sf3b1*$^{+/-}$ embryos. While Zfp144- or Rnf2-associated Sf3b1 were clearly decreased in *Sf3b1*$^{+/-}$ embryos, Rnf2 was precipitated equally in both embryos (Fig. 3C). It was also notable

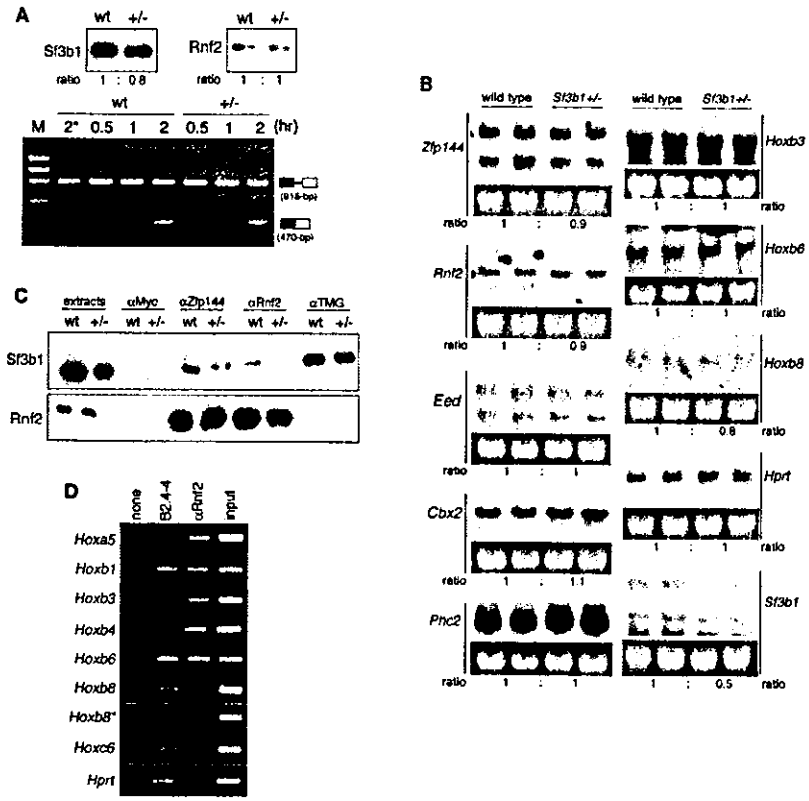

Figure 3. Comparison of wild-type and *Sf3b1*$^{+/-}$ embryos. Genotyping of embryos was performed with total DNA from yolk sacs. (*A*) In vitro splicing assay. The soluble fraction of a nuclear extract was prepared from wild-type or *Sf3b1*$^{+/-}$ embryos at 10.5 dpc. Equal amounts (60 µg) of total protein were confirmed by Western blotting with anti-Sf3b1 and anti-Rnf2 antibodies (*upper* panels) and subjected to a splicing assay (*lower* panel). One-step RT–PCR revealed that unspliced forms consisting of two exons and an intron (upper bands) as the RNA substrates were converted into spliced forms (lower bands) by the splicing reaction. Band intensities were measured by the image-processing program Image J and the ratios of *Sf3b1*$^{+/-}$ to wild type were obtained. (*B*) Northern analysis of total RNAs (15 µg each) from independent embryos at 12.5 dpc. Ethidium-bromide-stained 28S rRNAs prior to transfer to membranes are displayed *below* their blots. Intensity of each detected band was normalized by their rRNAs and then the ratios of *Sf3b1*$^{+/-}$ to wild type were calculated (indicated *below* their panels). (*C*) Immunoprecipitation assay with embryos at 11.5 dpc. Three independent embryos with the same genotype were sonicated individually, and the soluble lysates were mixed and then divided into four. Each was immunoprecipitated with a specific antibody. (*D*) ChIP assay with ES cells. Cross-linked chromatins were immunoprecipitated with or without indicated antibodies and subjected to amplification of *Hox* and *Hprt* regions (260–480 bp) by PCR. The amplified regions were detected in 1.5% agarose gels.

that the anti-TMG precipitates contained almost equal levels of Sf3b1, suggesting that the majority of U2 snRNP were not significantly altered in *Sf3b1*$^{+/-}$ embryos. This finding agrees well with the normal expression of other genes described above. Therefore, the heterozygous loss of *Sf3b1* gene results in significant reduction of Sf3b1 associated with PcG complexes, strongly suggesting a repressive mechanism of *Hox* genes via interaction with PcG complexes.

We finally examined whether Sf3b1 is closely associated to *Hox* genomic regions together with PcG proteins by chromatin immunoprecipitation (ChIP) assay. Various *Hox* cluster genes, including *Hoxa5*, *Hoxb1*, *Hoxb3*, *Hoxb4*, *Hoxb6*, *Hoxb8*, *Hoxb9*, and *Hoxc6*, were depressed in *Rnf2*$^{-/-}$ ES cells, indicating the involvement of PcG proteins in regulation of *Hox* expressions in ES cells (de Napoles et al. 2004; K. Isono and H. Koseki, unpubl.). Accordingly, we found obvious immunoprecipitation of 5′ genomic regions (260–480 bp) of *Hoxa5*, *Hoxb1*, *Hoxb3*, *Hoxb4*, *Hoxb6*, *Hoxb8*, and *Hoxc6* in wild-type ES cells by anti-Rnf2 antibody but not *Hprt* gene, which is not derepressed in *Rnf2*$^{-/-}$ ES cells (Fig. 3D). Likewise, we found association of Zfp144 to these *Hox* genes (K. Isono and H. Koseki, unpubl.). Anti-Sf3b1 antibody also precipitated a significant amount of 5′ genomic regions of these *Hox* genes while either anti-Rnf2 or anti-Sf3b1 antibody failed to precipitate the second exonic region of *Hoxb8* gene (indicated by *Hoxb8** in Fig. 3D). These findings indicate that the Sf3b1 and PcG proteins colocalize locally on the 5′ regions of individual *Hox* genes. It is also noteworthy that the relative degree of Sf3b1 association in comparison with the Rnf2 is greater at the *Hoxb6*, *Hoxb8*, and *Hoxc6* genomic regions than the *Hoxa5*, *Hoxb3*, and *Hoxb4* genes. This is in good agreement with another observation in *Sf3b1*$^{+/-}$ embryos that the expression of *Hoxb6*, *Hoxb8*, and *Hoxc6* was derepressed but not the *Hoxa5*, *Hoxb3*, or *Hoxb4* (summarized in Fig. 2R). Taken together, these results show that it is likely that a mechanistic link between Sf3b1 and PcG complexes regulates *Hox* gene expression via direct binding to *Hox* genomic regions.

Our results show a significant and novel mechanistic link between Sf3b1 (together probably with other U2 snRNP components) and PcG repressive complexes on *Hox* loci. This idea is strongly supported by our recent observation that heterozygous mutant mice for *Sf3b2*, another U2 snRNP component, exhibited skeletal abnormality similar to *Sf3b1* phenotypes: 10 out of 14 targeting mice (71%) had L6 to S1 transformation compared with two out of 18 wild-type mice (11%) (K. Isono and H. Koseki, unpubl.). However, although with respect to the PcG-mediated repression in the transcriptional-competent regions, our findings are in general accord with previous reports (Breiling et al. 2001; Saurin et al. 2001; King et al. 2002; Cmarko et al. 2003; de Graaff et al. 2003; Dellino et al. 2004), nevertheless they indicate the presence a different gene silencing mechanism. Evidence that the level of Sf3b1 in PcG complexes affects the expressional boundary of *Hox* genes implies that Sf3b1 supports the activity of PcG complexes. The simplest explanation is that Sf3b1/U2 snRNP might be a PcG protein and could form repressive PcG complexes together with other PcG proteins. A more interesting hypothesis is that this interaction constitutes part of a mechanism that is designed to maintain the amount of *Hox* transcripts required to confer the appropriate positional identities. Regulation of *Hox* expressions in the vicinity of their boundaries is thought to be loose, because even wild type occasionally exhibits homeotic transformations (Table 1 and Akasaka et al. 1996). RNAs, mistranscribed beyond loose repression, may be tethered by Sf3b1/U2 snRNP bound to PcG complex, leading to the arrest of splicing and a normal *Hox* boundary as a consequence. However, in *Sf3b1*$^{+/-}$ cells, because of the decrease of PcG complex-bound Sf3b1, such mistranscribed RNAs become easily associated with splicing-active nucleoplasmic Sf3b1/U2 snRNP. This association leads to the achievement of a splicing reaction, which results in the anterior shift of *Hox* expression. In support of this model is the important evidence that the *Mll* mutation completely suppressed *Sf3b1* phenotypes, indicating that the PcG-like function of Sf3b1 is very susceptible to levels of Mll; in other words the acting points of both proteins are spatially very close. Of further note is the fact that the human MLL supercomplex includes the 116-kDa protein specific to the U5 snRNP, which acts on pre-mRNA following the U2 snRNP (Nakamura et al. 2002). Finally, it appears that there are multiple interacting surfaces between PcG complexes and gene expression machineries. It might be that, through this interaction, PcG complexes act as a part of the modules that sense the transcriptional status in transcriptional-competent regions of the *Hox* cluster.

Materials and methods

Yeast two-hybrid screening, immunoprecipitation and GST pull-down assays, ChIP analysis, in vitro splicing assay, and knockout mice are described in the Supplemental Material.

Acknowledgments

We thank Drs. Miguel Vidal and Tsukasa Oda for providing *Rnf2* cDNA and pBTM116, respectively. In addition, we thank Drs. Takeshi Akasaka and Tomomi Kaneko, Ms. Kazumi Nemoto, Minako Ogawa, Misao Uchida, and Sanae Takeda for help with this work, and Drs. Achim Gossler and Miguel Vidal for their critical reading of the manuscript. This study was supported by Special Coordination Funds for Promoting Science and Technology from the Ministry of Education, Culture, Sports, Science and Technology, the Japanese Government.

References

Akasaka, T., Kanno, M., Balling, R., Mieza, M.A., Taniguchi, M., and Koseki, H. 1996. A role for *Mel18*, a *Polycomb* group-related vertebrate gene, during the anteroposterior specification of the axial skeleton. *Development* **122:** 1513–1522.

Akasaka, T., van Lohuizen, M., van der Lugt, N., Mizutani-Koseki, Y., Kanno, M., Taniguchi, M., Vidal, M., Alkema, M., Berns, A., and Koseki, H. 2001. Mice doubly deficient for the Polycomb Group genes *Mel18* and *Bmi1* reveal synergy and requirement for maintenance but not initiation of *Hox* gene expression. *Development* **128:** 1587–1597.

Bel, S., Core, N., Djabali, M., Kieboom, K., van der Lugt, N., Alkema, M.J., and van Lohuizen, M. 1998. Genetic interactions and dosage effects of Polycomb group genes in mice. *Development* **125:** 3543–3551.

Breiling, A., Turner, B. M., Bianchi, M. E., and Orlando, V. 2001. General transcription factors bind promoters repressed by Polycomb group proteins. *Nature* **412:** 651–655.

Cmarko, D., Verschure, P.J., Otte, A.P., van Driel, R., and Fakan, S. 2003. Polycomb group gene silencing proteins are concentrated in the perichromatin compartment of the mammalian nucleus. *J. Cell Sci.* **116:** 335–343.

de Graaff, W., Tomotsune, D., Oosterveen, T., Takihara, Y., Koseki, H., and Deschamps, J. 2003. Randomly inserted and targeted Hox/reporter fusions transcriptionally silenced in Polycomb mutants. *Proc. Natl. Acad. Sci.* **100:** 13362–13367.

Dellino, G.I., Schwartz, Y.B., Farkas, G., McCabe, D., Elgin, S.C.R., and Pirrotta, V. 2004. Polycomb silencing blocks transcription initiation. *Mol. Cell* **13:** 887–893.

de Napoles, M., Mermoud, J.E., Wakao, R., Tang, Y.A., Endoh, M., Appanah, R., Nesterova, T.B., Silva, J., Otte, A.P., Vidal, M., et al. 2004. Polycomb group proteins Ring1A/B link ubiquitylation of histone H2A to heritable gene silencing and X inactivation. *Dev. Cell* **7:** 663–676.

Duboule, D. and Morata, G. 1994. Colinearity and functional hierarchy among genes of the homeotic complexes. *Trends Genet.* **10:** 358–364.

Francis, N.J. and Kingston, R.E. 2001. Mechanisms of transcriptional memory. *Nat. Rev. Mol. Cell Biol.* **2:** 409–421.

Francis, N.J., Saurin, A.J., Shao, Z., and Kingston, R.E. 2001. Reconstitution of a functional core Polycomb repressive complex. *Mol. Cell* **8:** 545–556.

Gould, A. 1997. Functions of mammalian Polycomb group and trithorax group related genes. *Curr. Opin. Genet. Dev.* **7:** 488–494.

Hanson, R.D., Hess, J.L., Yu, B.D., Ernst, P., van Lohuizen, M., Berns, A., van der Lugt, M.N.T., Shashikant, C.S., Ruddle, F.H., Seto, M., et al. 1999. Mammalian *Trithorax* and *Polycomb*-group homologues are antagonistic regulators of homeotic development. *Proc. Natl. Acad. Sci.* **96:** 14372–14377.

Isono, K., Abe, K., Tomaru, Y., Okazaki, Y., Hayashizaki, Y., and Koseki, H. 2001. Molecular cloning, genetic mapping, and expression of the mouse Sf3b1 (SAP155) gene for the U2 snRNP component of spliceosome. *Mamm. Genome* **12:** 192–198.

King, I.F.G., Francis, N.J., and Kingston, R.E. 2002. Native and recombinant Polycomb group complexes establish a selective block to template accessibility to repress transcription in vitro. *Mol. Cell. Biol.* **22:** 7919–7928.

Krämer, A. 1996. The structure and function of proteins involved in mammalian pre-mRNA splicing. *Annu. Rev. Biochem.* **65:** 367–409.

McGinnis, W. and Krumlauf, R. 1992. Homeobox genes and axial patterning. *Cell* **68:** 283–302.

Nakamura, T., Mori, T., Tada, S., Krajewski, W., Rozovskaia, T., Wassell, R., Dubois, G., Mazo, A., Croce, C.M., and Canaani, E. 2002. ALL-1 is a histone methyltransferase that assembles a supercomplex of proteins involved in transcriptional regulation. *Mol. Cell* **10:** 1119–1128.

Orlando, V. 2003. Polycomb, epigenomes, and control of cell identity. *Cell* **112:** 599–606.

Satijn, D.P.E. and Otte, A.P. 1999. Polycomb group protein complexes: Do different complexes regulate distinct target genes? *Biochim. Biophys. Acta* **1447:** 1–16.

Saurin, A.J., Shao Z., Erdjument-Bromage, H., Tempst, P., and Kingston R.E. 2001. A *Drosophila* Polycomb group complex includes Zeste and dTAFII proteins. *Nature* **412:** 655–660.

Schmidt-Zachmann, M.S., Knecht, S., and Krämer, A. 1998. Molecular characterization of a novel, widespread nuclear protein that colocalizes with spliceosome components. *Mol. Biol. Cell* **9:** 143–160.

Shao, Z. Raible, F., Mollaaghababa, R., Guyon, J.R., Wu, C.-T., Bender, W., and Kingston, R.E. 1999. Stabilization of chromatin structure by PRC1, a Polycomb complex. *Cell* **98:** 37–46.

Simon J.A. and Tamkun, J.W. 2002. Programming off and on states in chromatin: Mechanisms of Polycomb and trithorax group complexes. *Curr. Opin. Genet. Dev.* **12:** 210–218.

Suzuki, M., Mizutani-Koseki, Y., Fujimura, Y., Miyagishima, H., Kaneko, T., Takada, Y., Akasaka, T., Tanzawa, H., Takihara, Y., Nakano, M., et al. 2002. Involvement of the Polycomb-group gene Ring1B in the specification of the anterior-posterior axis in mice. *Development* **129:** 4171–4183.

Yagi, H., Deguchi, K., Aono, A., Tani, Y., Kishimoto, T., and Komori, T. 1998. Growth disturbance in fetal liver hematopoiesis of MLL-mutant mice. *Blood* **92:** 108–117.

Yu, B.D., Hess, J.L., Horning, S.E., Brown, G.A., and Korsmeyer, S.J. 1995. Altered Hox expression and segmental identity in Mll-mutant mice. *Nature* **378:** 505–508.

事務局

中村　洋子

千葉県がんセンター研究所

〒260-8717　千葉市中央区仁戸名町666-2

電話　043-264-5431　/　FAX　043-265-4459